We recently reported that mechanical stress activates the AT_1 receptor independently of AngII and that this AngII-independent activation of AT_1 receptor is inhibited by the inverse agonist, candesartan.[6] Therefore, we next examined the inhibitory effects of olmesartan on stretch-induced ERK activation in cardiomyocytes cultured from neonatal rats. We found that the stretch-induced phosphorylation of ERKs in cultured cardiomyocytes was largely dependent on the direct activation of AT_1 receptor and that AngII, even if secreted from cardiomyocytes, had only a marginal role in the stretch-induced activation of ERKs.[6] We found that the activation of ERKs in response to mechanical stretch was significantly attenuated by a pretreatment with 10^{-7} M olmesartan (Figure 4a). Furthermore, to exclude the effect of secreted AngII on stretch-induced ERK activation, we imposed stretch stimulation on HEK293 cells that showed no detectable expression of angiotensinogen.[6] Neither stimulation with AngII nor mechanical stretch activated ERKs in HEK293 cells, but mechanical stretching did activate ERKs in these cells when the AT_1 receptor was overexpressed[6] (Figure 4b). Similar to the results in cardiomyocytes, pretreatment with olmesartan significantly inhibited stretch-induced ERK activation in HEK293 cells expressing the AT_1 receptor (HEK293-AT_1 cells) (Figure 4b). Furthermore, the inhibitory effect of olmesartan on stretch-induced ERK activation was significantly stronger than that of losartan (Figure 5). These results suggest that olmesartan, as a potent inverse agonist, strongly suppresses stretch-induced ERK activation, as well as the basal activity of the AT_1 receptor.

We further examined the inhibitory effects of R-239470 and R-90929 on stretch-induced ERK activation, both in cardiomyocytes and in HEK293-AT_1 cells. As shown in Figure 4, 10^{-7} M R-239470 or R-90929 could not inhibit ERK activation induced either by 10^{-7} M AngII or by mechanical stretch, although 10^{-7} M olmesartan inhibited ERK activation. Interestingly, AngII-induced ERK activation was inhibited by 10^{-5} M R-239470 and 10^{-6} M R-90929, but stretch-induced ERK activation was not inhibited by the same concentrations of these compounds (Figure 4). These results suggest that the carboxyl and the hydroxyl groups present in olmesartan are responsible for the potent inverse agonist activity olmesartan exerts against stretch-induced ERK activation. Similar to the results of experiments evaluating stretch-induced ERK activation, 10^{-5} M R-239470 and 10^{-6} M R-90929 failed to suppress basal *c-fos* promoter activity in HEK293 cells expressing AT_1-N111G (Figure 2).

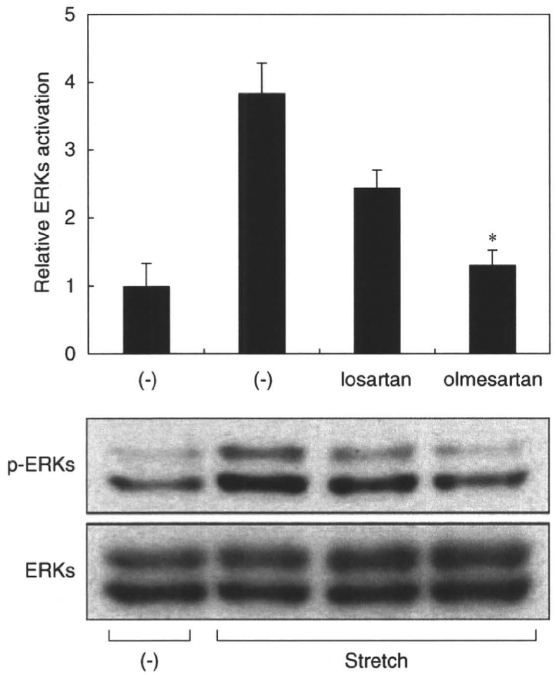

Figure 5 Comparison of the inverse agonist activities of olmesartan and losartan against stretch-induced ERK activation. HEK293-AT_1 cells were stimulated by mechanical stretch, and the activation of extracellular signal-regulated protein kinase (ERKs) was determined. The inhibitory effect of 10^{-7} M olmesartan on stretch-induced ERK activation was much stronger than that of 10^{-7} M losartan. *$P<0.01$ *vs.* that of losartan. AT_1, angiotensin II type 1.

Inhibitory effects of olmesartan on stretch-induced ERK activation in mutated AT_1 receptors

Structure–function analyses have shown that ternary interactions between the hydroxyl group of olmesartan and Tyr^{113} of the AT_1 receptor and between the carboxyl group of olmesartan and Lys^{199} and His^{256} of the AT_1 receptor are essential for the inverse agonist activity that olmesartan exerts on basal IP production in both AT_1-WT and AT_1-N111G receptors.[9] The tetrazole group of olmesartan also interacts with Gln^{257} of the AT_1 receptor, but its binding is not required to reduce the basal activity level of the AT_1 receptor.[9] We first examined the effect of olmesartan on stretch-induced ERK activation in HEK293 cells overexpressing AT_1-WT or an AT_1 mutant receptor harboring one of the following mutations: Y113F, K199Q, H256A or Q257A. As shown in Figure 6a, mechanical stretch-induced phosphorylation of ERKs occurred in AT_1-Y113F, AT_1-K199Q, AT_1-H256A and AT_1-Q257A cells in degrees equivalent to AT_1-WT cells. Interestingly, the inhibitory effects of olmesartan on stretch-induced ERK activation were abolished in cells expressing AT_1-Y113F, AT_1-K199Q, AT_1-H256A or AT_1-Q257A (Figure 6a). These results suggest that the interactions between olmesartan and Gln^{257}, Tyr^{113}, Lys^{199} and His^{256} are required for the potent inverse agonism olmesartan exerts on stretch-induced activation of the AT_1 receptor.

As the tetrazole ring of olmesartan interacts with Gln^{257} of the AT_1 receptor,[9] we next examined the inhibitory effect that R-88145 (in which the tetrazole group was replaced with a carboxyl group, Figure 6b) had on stretch-induced ERK activation in HEK293 cells overexpressing AT_1-WT. Although 10^{-7} M R-88145 did not inhibit ERK activation induced by 10^{-7} M AngII, 10^{-5} M R-88145 could inhibit ERK activation to an extent equivalent to 10^{-7} M olmesartan (Figure 6c). However, stretch-induced ERK activation was not significantly inhibited by 10^{-5} M R-88145 (Figure 6c). These results suggest that the interaction between the tetrazole group of olmesartan and Gln^{257} of the AT_1 receptor is also responsible for the potent inverse agonist activity olmesartan exerts against stretch-induced ERK activation.

DISCUSSION

The ARBs share a common mode of action, namely they block AngII-mediated responses, but the antihypertensive potency of ARBs differs by drug.[2,4] Indeed, the pharmacokinetics of ARBs in human bodies, specifically factors such as bioavailability, half-life duration and route of elimination, differ considerably between different ARBs. These different degrees of efficacy possessed by ARBs are based on differences in their chemical structures, which determine their unique pharmacological properties. Insurmountable antagonism is one of the pharmacological parameters that is relevant to antihypertensive efficacy.[11] Insurmountable antagonism reflects tight binding and a slow dissociation of the drug–receptor complex. ARBs with insurmountable

antagonist properties suppress maximal AngII-induced responses.[11] Recently, it was reported that olmesartan showed a higher degree of insurmountable antagonism than did telmisartan against AngII-induced IP accumulation in CHO-K1 cells expressing the AT_1 receptor.[12] In this study, we showed that olmesartan shows insurmountable antagonist activity against the AT_1 receptor and that the carboxyl and hydroxyl groups on the imidazole ring are required for the insurmountable inhibition of AngII-induced ERK activation and *c-fos* gene expression (Figure 1).

The unique side-chain structure olmesartan possesses (its carboxyl group and hydroxyl group) contributes to its specific receptor-binding activity. These drug–receptor interactions cooperate to stabilize the receptor in an inactive conformation and thereby confer inverse agonism against the basal expression of the *c-fos* gene (Figure 2) and the basal production of IP[9] in cells expressing the AT_1-N111G receptor, as well as insurmountable antagonism. The inverse agonist activities that ARBs exert against the constitutive activity of the AT_1 receptor could be an important pharmacological parameter that may be relevant to their efficacy at blood pressure lowering and in preventing end-organ damage. Although it remains unclear whether the subtle constitutive activity of the native AT_1 receptor has a pathophysiological role, the enhancement of its constitutive activity

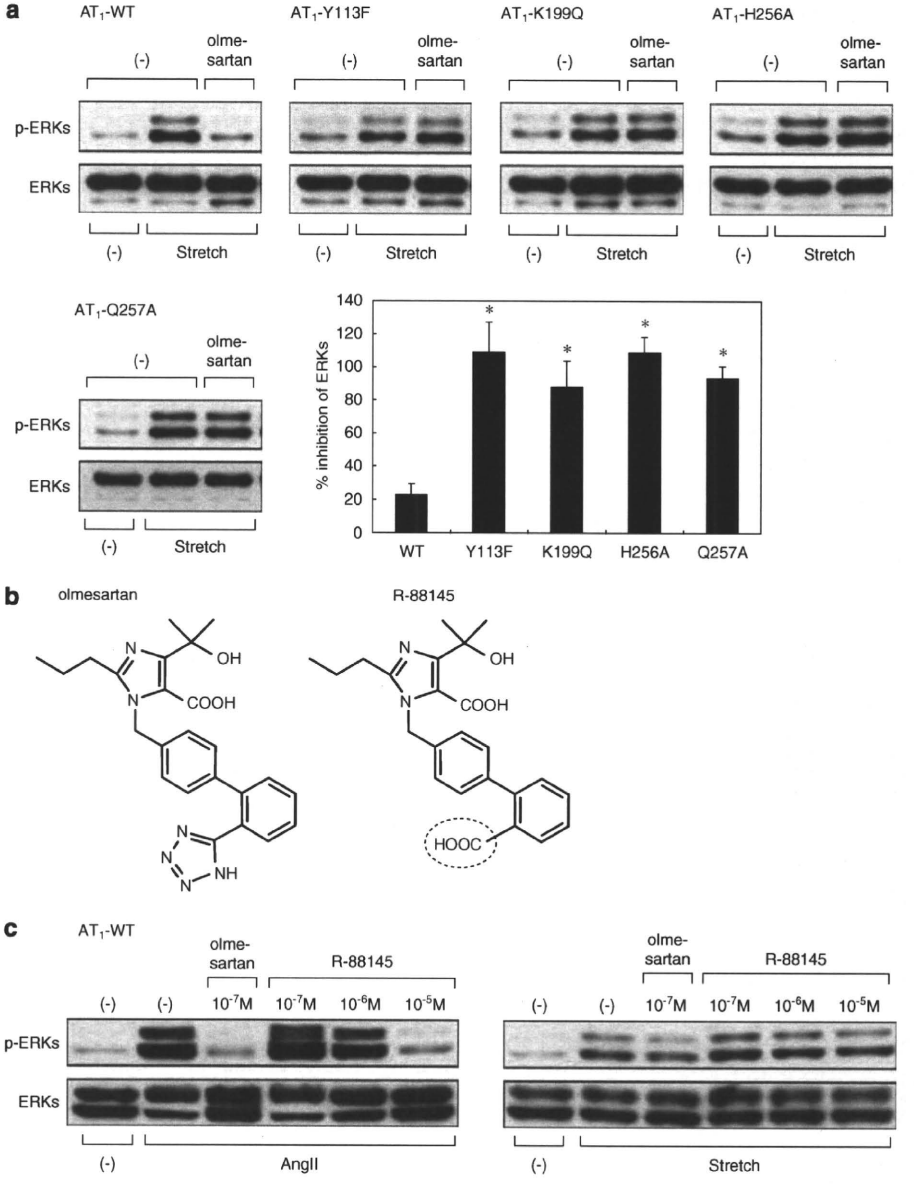

Figure 6 Specific drug–receptor interactions are required for olmesartan's inverse agonist activity against stretch-induced extracellular signal-regulated protein kinase (ERK) activation. (**a**) HEK293 cells expressing AT_1-WT, -Y113F, -K199Q, -H256A or -Q257A mutant receptors were pretreated with 10^{-7} M olmesartan and stimulated by mechanical stretch. The activation of ERKs was then determined. *$P<0.01$ *vs.* that of wild-type AT_1-WT. (**b**) The chemical structures of olmesartan and R-88145, which has a carboxyl group (circled COOH) instead of a tetrazole group. (**c**) HEK293-AT_1 cells were pretreated with indicated concentrations of olmesartan or R-88145 and were stimulated by 10^{-7} M AngII (left) or mechanical stretch (right). The activation of ERKs was then determined. AT_1, angiotensin II type 1.

through upregulation of receptor expression may promote cardiovascular remodeling. Indeed, the expression level of the AT_1 receptor in vascular cells is upregulated by low-density lipoprotein cholesterol,[13] insulin,[14] glucose,[15] progesterone[16] and inflammatory cytokines, such as interleukin-1α or interleukin-6.[17,18] Analyses of the binding affinity of olmesartan for mutant AT_1 receptors as well as molecular modeling analyses indicated that the ternary interactions between the hydroxyl group and Tyr^{113} and between the carboxyl group and Lys^{199} and His^{256} are critical to the inverse agonist properties of olmesartan, but that the interaction between the tetrazole group and Gln^{257} is dispensable.[9] Interestingly, differential interactions between valsartan and Ser^{105}, and between Ser^{109} and Lys^{199}, are crucial for producing inverse agonism.[19] It has therefore been proposed that ARBs may bind to the AT_1 receptor primarily by docking at Lys^{199} and subsequently through a distinct combination of drug–receptor interactions in a drug-specific manner.[19] According to this model, the spatial pattern of drug–receptor contact points will determine the potency of the inverse agonist activity of a given ARB.

We recently showed that mechanical stretching of cells induces a counterclockwise rotation and a shift of TM7 of the AT_1 receptor toward the ligand-binding pocket.[7] However, TM7 shifts away from the ligand-binding pocket in the AT_1-N111G receptor,[10] implying that the conformation of AT_1 receptor during stretch-induced activation is different from that of the constitutively active AT_1 receptor. In general, GPCRs are structurally flexible and unstable, and multiple conformational states exist during the GPCR activation process.[20–22] In this study, we showed that, aside from the ternary drug–receptor interactions involving the hydroxyl and carboxyl groups of olmesartan, an additional interaction between the tetrazole group of olmesartan and Gln^{257} of the AT_1 receptor is required for its potent inverse agonism against stretch-induced AT_1 receptor activation (Figures 4 and 6). Each of the quaternary interactions involving the hydroxyl group, carboxyl group and tetrazole group contributes to a tight drug–receptor binding,[9] but is not sufficient enough to produce a potent inverse agonism against stretch-induced AT_1 receptor activation. Thus, the quaternary drug–receptor interactions work together to stabilize the receptor in an inactive conformation, even under conditions in which mechanical stretching occurs.

With regard to candesartan, the carboxyl group on the benzimidazole ring is responsible for its inverse agonism and leads to the suppression of both the constitutive activity and the mechanical stress-induced activation of the AT_1 receptor.[7] The SCAM studies showed that the binding of the carboxyl group of candesartan to Gln^{257} of TM6 and Thr^{287} of TM7 forcibly induces a clockwise rotation of TM6 and TM7, and leads to the stabilization of the AT_1 receptor in an inactive conformation.[7] At present, it remains unclear how the helical movement of TM7 induced by mechanical stretch is affected by the presence of olmesartan. According to molecular modeling, Thr^{287} of TM7 is located in a position that would allow it to form a hydrogen bond with His^{256} of TM6.[9] We assume that the helical movements of TM6 and TM7 are coupled and that TM7 may be restricted in motion when TM6 is rigidly bound to olmesartan through the dual interactions between the carboxyl group and His^{256} and between the tetrazole group of olmesartan and Gln^{257}.

Our study shows that olmesartan strongly inhibits both AngII-dependent and AngII-independent activation of the AT_1 receptor. Ternary drug–receptor interactions between the hydroxyl group and Tyr^{113} and between the carboxyl group and Lys^{199} and His^{256} are crucial for olmesartan's inverse agonist activity against the constitutive activity of an AT_1 mutant receptor, AT_1-N111G. In addition, a drug–receptor interaction between the tetrazole group of olmesartan and Gln^{257} of the AT_1 receptor is required for potent inverse agonism against stretch-induced AT_1 receptor activation. These results suggest that multivalent drug–receptor interactions cooperate in combination to stabilize the receptor in an inactive conformation according to the distinct processes of receptor activation. The inverse agonist activity of ARBs has therapeutic benefits in the prevention of load-induced cardiac hypertrophy,[5] and thus has the potential to affect long-term outcomes in patients with hypertension. Elucidation of the molecular basis for the inverse agonist activity of ARBs in relation to their chemical structure will help to categorize ARBs according to their individual efficacies in receptor inactivation and will also help researchers to develop novel ARBs with superb efficacy in terms of blood pressure lowering and end-organ protection.

CONFLICT OF INTEREST

The authors declare no conflict of interest.

ACKNOWLEDGEMENTS

We thank A Furuyama, M Ikeda, Y Ohtsuki and I Sakamoto for their excellent technical assistance. This work was supported in part by grants from the Japanese Ministry of Education, Science, Sports, and Culture, as well as Health and Labor Sciences Research Grants (to IK and HA). Additional grants from the Japan Intractable Diseases Research Foundation, the Kowa Life Science Foundation and the Takeda Science Foundation (to HA) were used to support this research.

1 de Gasparo M, Catt KJ, Inagami T, Wright JW, Unger T. International union of pharmacology. XXIII. The angiotensin II receptors. *Pharmacol Rev* 2000; **52**: 415–472.
2 Zaman MA, Oparil S, Calhoun DA. Drugs targeting the renin-angiotensin-aldosterone system. *Nat Rev Drug Discov* 2002; **1**: 621–636.
3 Kjeldsen SE, Dahlof B, Devereux RB, Julius S, Aurup P, Edelman J, Beevers G, de Faire U, Fyhrquist F, Ibsen H, Kristianson K, Lederballe-Pedersen O, Lindholm LH, Nieminen MS, Omvik P, Oparil S, Snapinn S, Wedel H. Effects of losartan on cardiovascular morbidity and mortality in patients with isolated systolic hypertension and left ventricular hypertrophy: a Losartan Intervention for Endpoint Reduction (LIFE) substudy. *JAMA* 2002; **288**: 1491–1498.
4 Oparil S. Newly emerging pharmacologic differences in angiotensin II receptor blockers. *Am J Hypertens* 2000; **13**: 18S–24S.
5 Akazawa H, Yasuda N, Komuro I. Mechanisms and functions of agonist-independent activation in the angiotensin II type 1 receptor. *Mol Cell Endocrinol* 2009; **302**: 140–147.
6 Zou Y, Akazawa H, Qin Y, Sano M, Takano H, Minamino T, Makita N, Iwanaga K, Zhu W, Kudoh S, Toko H, Tamura K, Kihara M, Nagai T, Fukamizu A, Umemura S, Iiri T, Fujita T, Komuro I. Mechanical stress activates angiotensin II type 1 receptor without the involvement of angiotensin II. *Nat Cell Biol* 2004; **6**: 499–506.
7 Yasuda N, Miura S, Akazawa H, Tanaka T, Qin Y, Kiya Y, Imaizumi S, Fujino M, Ito K, Zou Y, Fukuhara S, Kunimoto S, Fukuzaki K, Sato T, Ge J, Mochizuki N, Nakaya H, Saku K, Komuro I. Conformational switch of angiotensin II type 1 receptor underlying mechanical stress-induced activation. *EMBO Rep* 2008; **9**: 179–186.
8 Milligan G. Constitutive activity and inverse agonists of G protein-coupled receptors: a current perspective. *Mol Pharmacol* 2003; **64**: 1271–1276.
9 Miura S, Fujino M, Hanzawa H, Kiya Y, Imaizumi S, Matsuo Y, Tomita S, Uehara Y, Karnik SS, Yanagisawa H, Koike H, Komuro I, Saku K. Molecular mechanism underlying inverse agonist of angiotensin II type 1 receptor. *J Biol Chem* 2006; **281**: 19288–19295.
10 Boucard AA, Roy M, Beaulieu ME, Lavigne P, Escher E, Guillemette G, Leduc R. Constitutive activation of the angiotensin II type 1 receptor alters the spatial proximity of transmembrane 7 to the ligand-binding pocket. *J Biol Chem* 2003; **278**: 36628–36636.
11 Van Liefde I, Vauquelin G. Sartan-AT(1) receptor interactions: in vitro evidence for insurmountable antagonism and inverse agonism. *Mol Cell Endocrinol* 2009; **302**: 237–243.
12 Le MT, Pugsley MK, Vauquelin G, Van Liefde I. Molecular characterisation of the interactions between olmesartan and telmisartan and the human angiotensin II AT1 receptor. *Br J Pharmacol* 2007; **151**: 952–962.
13 Nickenig G, Jung O, Strehlow K, Zolk O, Linz W, Scholkens BA, Bohm M. Hypercholesterolemia is associated with enhanced angiotensin AT1-receptor expression. *Am J Physiol* 1997; **272**: H2701–H2707.

14 Nickenig G, Roling J, Strehlow K, Schnabel P, Bohm M. Insulin induces upregulation of vascular AT1 receptor gene expression by posttranscriptional mechanisms. *Circulation* 1998; **98**: 2453–2460.
15 Sodhi CP, Kanwar YS, Sahai A. Hypoxia and high glucose upregulate AT1 receptor expression and potentiate ANG II-induced proliferation in VSM cells. *Am J Physiol Heart Circ Physiol* 2003; **284**: H846–H852.
16 Nickenig G, Strehlow K, Wassmann S, Baumer AT, Albory K, Sauer H, Bohm M. Differential effects of estrogen and progesterone on AT(1) receptor gene expression in vascular smooth muscle cells. *Circulation* 2000; **102**: 1828–1833.
17 Sasamura H, Nakazato Y, Hayashida T, Kitamura Y, Hayashi M, Saruta T. Regulation of vascular type 1 angiotensin receptors by cytokines. *Hypertension* 1997; **30**: 35–41.
18 Wassmann S, Stumpf M, Strehlow K, Schmid A, Schieffer B, Bohm M, Nickenig G. Interleukin-6 induces oxidative stress and endothelial dysfunction by overexpression of the angiotensin II type 1 receptor. *Circ Res* 2004; **94**: 534–541.
19 Miura S, Kiya Y, Kanazawa T, Imaizumi S, Fujino M, Matsuo Y, Karnik SS, Saku K. Differential bonding interactions of inverse agonists of angiotensin II type 1 receptor in stabilizing the inactive state. *Mol Endocrinol* 2008; **22**: 139–146.
20 Gether U. Uncovering molecular mechanisms involved in activation of G protein-coupled receptors. *Endocr Rev* 2000; **21**: 90–113.
21 Miura S, Saku K, Karnik SS. Molecular analysis of the structure and function of the angiotensin II type 1 receptor. *Hypertens Res* 2003; **26**: 937–943.
22 Perez DM, Karnik SS. Multiple signaling states of G-protein-coupled receptors. *Pharmacol Rev* 2005; **57**: 147–161.

nature medicine

A crucial role for adipose tissue p53 in the regulation of insulin resistance

Tohru Minamino[1,2,7], Masayuki Orimo[1,7], Ippei Shimizu[1,7], Takeshige Kunieda[1], Masataka Yokoyama[1], Takashi Ito[1], Aika Nojima[1], Akira Nabetani[3], Yuichi Oike[2,4], Hisahiro Matsubara[5], Fuyuki Ishikawa[3] & Issei Komuro[1,6]

Various stimuli, such as telomere dysfunction and oxidative stress, can induce irreversible cell growth arrest, which is termed 'cellular senescence'[1,2]. This response is controlled by tumor suppressor proteins such as p53 and pRb. There is also evidence that senescent cells promote changes related to aging or age-related diseases[3–6]. Here we show that p53 expression in adipose tissue is crucially involved in the development of insulin resistance, which underlies age-related cardiovascular and metabolic disorders. We found that excessive calorie intake led to the accumulation of oxidative stress in the adipose tissue of mice with type 2 diabetes–like disease and promoted senescence-like changes, such as increased activity of senescence-associated β-galactosidase, increased expression of p53 and increased production of proinflammatory cytokines. Inhibition of p53 activity in adipose tissue markedly ameliorated these senescence-like changes, decreased the expression of proinflammatory cytokines and improved insulin resistance in mice with type 2 diabetes–like disease. Conversely, upregulation of p53 in adipose tissue caused an inflammatory response that led to insulin resistance. Adipose tissue from individuals with diabetes also showed senescence-like features. Our results show a previously unappreciated role of adipose tissue p53 expression in the regulation of insulin resistance and suggest that cellular aging signals in adipose tissue could be a new target for the treatment of diabetes.

Cellular senescence was originally defined as the finite replication of human somatic cells in culture. As a consequence of semiconservative DNA replication, the ends of the chromosomes (telomeres) are not duplicated completely, resulting in successive shortening of the telomeres with each cell division[7]. Telomerase is a ribonucleoprotein that adds telomeres to the ends of chromosomes. Telomeres that have shortened beyond a critical threshold, resulting in cell death or senescence, are thought to cause DNA damage that induces cellular senescence. It is now apparent that senescence can be induced by various stresses independently of cell replication, such as chromatin damage related to oxidative stress, and cellular senescence is believed to be a potent anticancer mechanism. Accumulating evidence also suggests a potential relationship between cellular senescence and aging of organisms[8,9].

Aging is known to increase the prevalence of metabolic disorders such as diabetes. Therefore, we hypothesized that cellular aging might influence insulin resistance and accelerate the development of diabetes. To test our hypothesis, we used Ay mice with ectopic expression of agouti peptide, which leads to perturbation of the central melanocortin pathway and thereby induces excessive calorie intake, resulting in obesity and diabetes. It has been reported that production of reactive oxygen species (ROS) is selectively increased in the adipose tissue of obese mice and that increased oxidative stress in fat is a key mechanism underlying the occurrence of insulin resistance related to obesity[10]. Consistent with previous studies, Ay mice on a normal diet for 20 weeks showed higher adipose tissue amounts of ROS compared with wild-type mice on the same diet (**Supplementary Fig. 1a**). Because increased stress due to ROS can induce DNA damage and subsequent activation of p53, leading to telomere-independent senescence[3,4], we tested whether adipose tissue of Ay mice shows a senescence-like phenotype. The adipose tissue of these mice showed senescence-like changes, including enhanced activity of senescence-associated β-galactosidase (SA-β-gal; **Fig. 1a**). Ay mice also showed higher adipose tissue amounts of p53 on the protein level and cyclin-dependent kinase inhibitor-1A (*Cdkn1a*) expression on the mRNA level compared to wild-type mice (**Fig. 1b,c**), suggesting excessive caloric intake can induce senescence-like changes in adipose tissue.

It has been reported that increased secretion of proinflammatory cytokines by adipose tissue exacerbates insulin resistance in people with metabolic disorders[11–13]. Senescent cells are known to secrete molecules that can alter the local microenvironment, such as proinflammatory cytokines[3,5]. We therefore speculated that senescence-like changes might be associated with increased expression of proinflammatory cytokines by adipose tissue that could induce insulin resistance. Consistent with this concept, expression of proinflammatory cytokines such as tumor necrosis factor-α (*Tnf*) and chemokine (C-C motif) ligand-2 (*Ccl2*), also known as monocyte chemoattractant protein-1, was upregulated in association with an increase

[1]Department of Cardiovascular Science and Medicine, Chiba University Graduate School of Medicine, Chuo-ku, Chiba, Japan. [2]PRESTO, Japan Science and Technology Agency, Saitama, Japan. [3]Department of Gene Mechanisms, Graduate School of Biostudies, Kyoto University, Yoshida-Konoe-cho, Kyoto, Japan. [4]Department of Molecular Genetics, Faculty of Medical and Pharmaceutical Sciences, Kumamoto University, Kumamoto, Japan. [5]Department of Frontier Surgery, Chiba University Graduate School of Medicine, Chuo-ku, Chiba, Japan. [6]Department of Cardiovascular Medicine, Osaka University Graduate School of Medicine, Suita, Osaka, Japan. [7]These authors contributed equally to this work. Correspondence should be addressed to I.K. (komuro-tky@umin.ac.jp).

Received 25 March; accepted 29 June; published online 30 August 2009; doi:10.1038/nm.2014

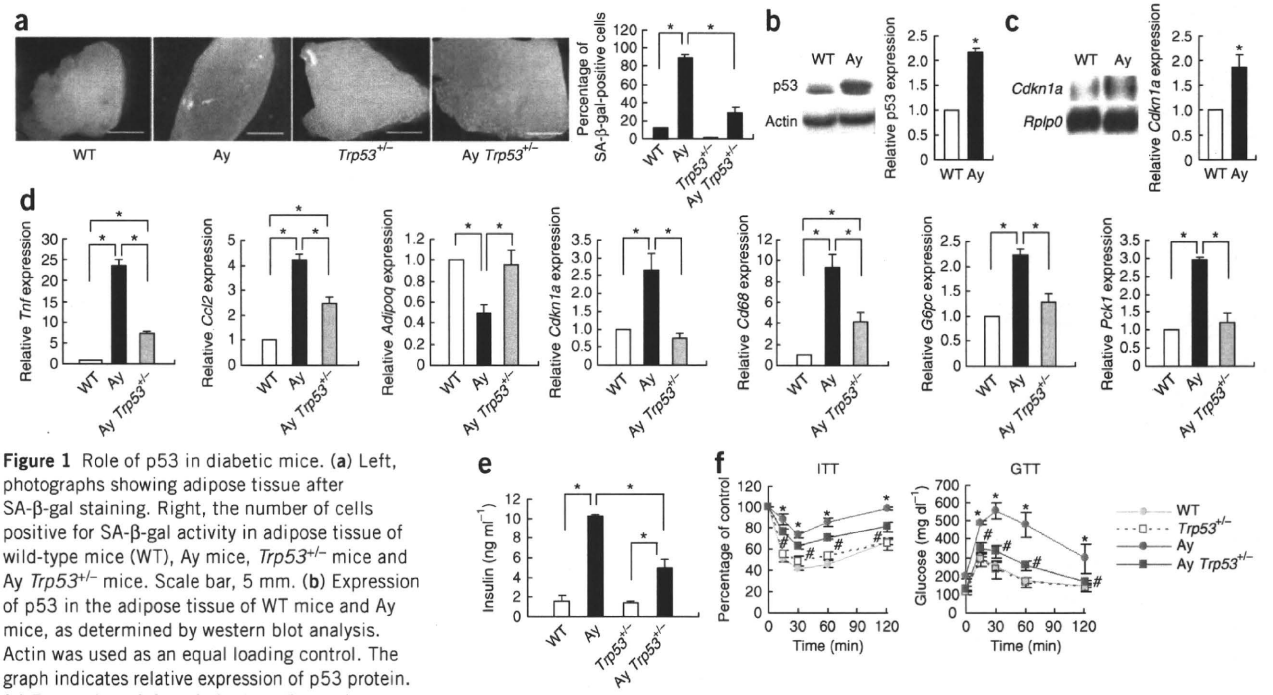

Figure 1 Role of p53 in diabetic mice. (**a**) Left, photographs showing adipose tissue after SA-β-gal staining. Right, the number of cells positive for SA-β-gal activity in adipose tissue of wild-type mice (WT), Ay mice, *Trp53*$^{+/-}$ mice and Ay *Trp53*$^{+/-}$ mice. Scale bar, 5 mm. (**b**) Expression of p53 in the adipose tissue of WT mice and Ay mice, as determined by western blot analysis. Actin was used as an equal loading control. The graph indicates relative expression of p53 protein. (**c**) Expression of *Cdkn1a* in the adipose tissue WT mice and Ay mice, as determined by northern blot analysis. Ribosomal protein, large, P0 (Rplp0) was used as an equal loading control. The graph indicates relative expression of *Cdkn1a* mRNA. (**d**) Real-time PCR assessing the expression of cytokines, *Cdkn1a* and *Cd68* in adipose tissue and the expression of *G6pc* (encoding glucose-6-phosphatase) and *Pck1* (encoding phosphoenolpyruvate carboxykinase) in the livers of WT mice, Ay mice and Ay *Trp53*$^{+/-}$ mice. (**e**) Plasma insulin concentrations in WT mice, Ay mice, *Trp53*$^{+/-}$ mice and Ay *Trp53*$^{+/-}$ mice. $^{*}P < 0.05$; $n = 4$–6 for **a** and **d**; $n = 3$ for **b**; $n = 4$ for **c** and **e**. (**f**) Insulin tolerance test (ITT) and glucose tolerance test (GTT) in WT mice, Ay mice, *Trp53*$^{+/-}$ mice and Ay *Trp53*$^{+/-}$ mice. $^{*}P < 0.05$ versus WT; $^{\#}P < 0.05$ versus Ay; $n = 7$. Data are shown as the means ± s.e.m.

of macrophage marker expression, whereas expression of anti-inflammatory cytokines (including adiponectin, (*Adipoq*)) was downregulated in the adipose tissue of Ay mice (**Fig. 1d**). We detected upregulation of inflammatory cytokines, as well as of p53 protein and *Cdkn1a* expression, in both the stromal vascular fraction (macrophage-rich fraction) and the adipose-rich fraction (**Supplementary Fig. 1b**), suggesting that senescence of both macrophages and adipocytes causes an inflammatory response that leads to insulin resistance.

We next investigated whether inhibition of p53 could reverse insulin resistance and glucose intolerance in Ay mice. The number of SA-β-gal–positive cells and the expression of *Cdkn1a* were significantly lower in adipose tissue from Ay *Trp53*$^{+/-}$ mice than in tissue from Ay *Trp53*$^{+/+}$ mice (**Fig. 1a,d**), whereas there was no significant difference in food intake between the two groups (**Supplementary Fig. 1c**). The fat weight of Ay *Trp53*$^{+/-}$ mice was slightly lower than that of Ay *Trp53*$^{+/+}$ mice (**Supplementary Fig. 2a**). Reduced activation of p53 led to lower plasma insulin concentrations in Ay mice and also to normalization of cytokine and macrophage marker expression by adipose tissue (**Fig. 1d,e**). Hepatic expression of gluconeogenic enzymes was also lower in Ay *Trp53*$^{+/-}$ mice (**Fig. 1d**). Consistent with these changes, Ay *Trp53*$^{+/-}$ mice showed significantly better insulin sensitivity and glucose tolerance compared with Ay *Trp53*$^{+/+}$ mice as determined by insulin and glucose tolerance tests (**Fig. 1f**).

Because Ay *Trp53*$^{+/-}$ mice have p53 haploinsufficiency throughout the whole body, improvement of insulin resistance might be attributable to inhibition of p53 activity in other tissues aside from the white adipose tissue. To investigate the role of adipose tissue p53 in the regulation of insulin resistance, we generated mice with adipocyte-specific p53 deficiency (adipo-p53–deficient mice), using transgenic mice that express Cre recombinase under control of the mouse fatty acid–binding protein-4 (*Fabp4*) promoter, and fed these mice a high-fat, high-sucrose (HF-HS) diet for 4 months. Expression of p53 protein and *Cdkn1a* mRNA in adipose tissue was significantly upregulated in littermate control mice on the HF-HS diet, whereas this increase was significantly attenuated in adipo-p53–deficient mice (*Trp53*$^{loxP/loxP}$ Fabp4-Cre) receiving the same diet (**Fig. 2a,b** and **Supplementary Fig. 1d**). These mice had a slightly smaller increase of fat weight (**Supplementary Fig. 2b**) and normalized expression of adipokines and hepatic gluconeogenic enzymes (**Fig. 2b**), whereas hepatic p53 protein expression was unchanged (**Fig. 2a**). Insulin-induced phosphorylation of Akt was also restored in adipo-p53–deficient mice (**Supplementary Fig. 1e**). Consequently, insulin resistance induced by the HF-HS diet was lower in mice with adipocyte-specific ablation of p53 compared to control mice (**Fig. 2c**), indicating that p53 expression in adipose tissue has a crucial role in the development of insulin resistance.

It has been reported that Fabp4 is expressed in hematopoietic cells and has considerable influence on various biological responses[14,15]. To examine the possible involvement of p53 in hematopoietic cells, we transplanted wild-type bone marrow cells into adipo-p53–deficient mice or littermate control mice and induced dietary obesity in these mice. Adipo-p53–deficient mice transplanted with wild-type bone marrow cells showed better glucose tolerance than littermate control mice transplanted with wild-type marrow cells, but their glucose tolerance was impaired compared with that of adipo-p53–deficient mice without bone marrow transplantation (**Supplementary Fig. 1f**). In adipose-p53–deficient mice, expression of p53 protein and *Cdkn1a* was considerably lower in both the stromal vascular fraction and the

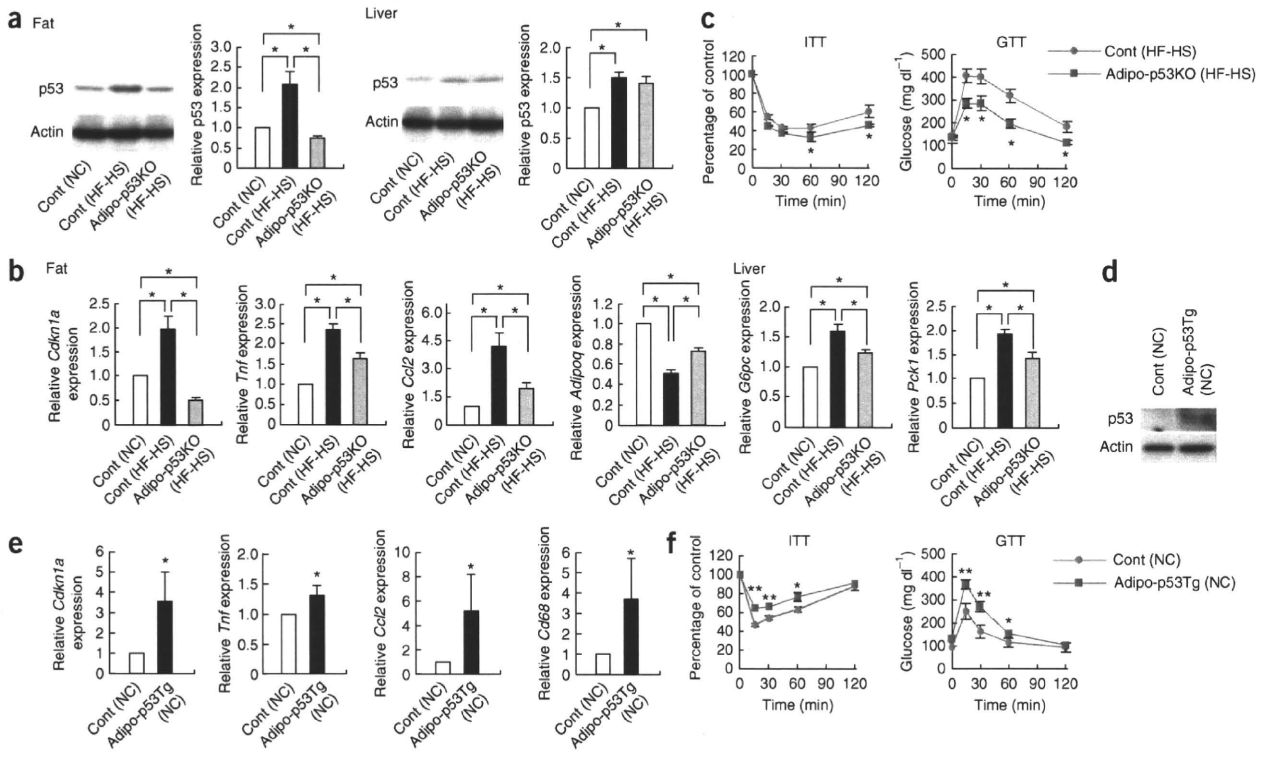

Figure 2 Adipose tissue p53 expression contributes to insulin resistance in mice with dietary obesity. (**a**) Western blot analysis for p53 in the fat and liver of littermate controls (Cont) on a normal diet (normal chow, NC), littermate controls (Cont) on an HF-HS diet (HF-HS), and adipo-p53–deficient mice (Adipo-p53KO) on an HF-HS diet (HF-HS). The graph indicates relative expression of p53 protein. (**b**) Real-time PCR assessing the expression of *Cdkn1a*, *Tnf*, *Ccl2* and *Adipoq* in adipose tissue and *G6pc* and *Pck1* in liver of the same mice as in **a**. $^*P < 0.05$; $n = 5$ mice for **a** and **b**. (**c**) ITT and GTT in Adipo-p53KO mice and littermate controls (Cont) after 4 months on a HF-HS diet or a normal diet. $^*P < 0.05$ versus control (HF-HS); $n = 8$. (**d**) Western blot analysis for p53 in adipose tissue of littermate controls (Cont) and adipo-p53–transgenic (Adipo-p53Tg) mice on a normal diet (NC). (**e**) Real-time PCR assessing the expression of *Cdkn1a*, *Tnf*, *Ccl2* and *Cd68* in adipose tissue of the same mice as in **d**. $^*P < 0.05$; $n = 5$. (**f**) ITT and GTT in Adipo-p53Tg mice and littermate controls (Cont) on a normal diet (NC). $^*P < 0.05$, $^{**}P < 0.01$ versus control; $n = 8$. Data are shown as the means ± s.e.m.

adipose-rich fraction compared with the levels seen in littermate control mice (**Supplementary Fig. 1d**). These results suggested that both macrophages and adipocytes contribute to the senescence-like changes of adipose tissues in mice with dietary obesity and that upregulation of p53 expression in adipose tissue has a pathological role in producing insulin resistance.

To further investigate the role of adipose tissue p53, we established transgenic mice that showed an increase of p53 protein and *Cdkn1a* mRNA expression in adipose tissue (**Fig. 2d,e**). Consistent with the results found in adipose-p53–deficient mice, these transgenic mice on a normal diet showed higher expression of proinflammatory cytokines and a macrophage marker (**Fig. 2e**), which was associated with impairment of insulin sensitivity and glucose tolerance (**Fig. 2f**), providing further evidence for a major role for adipose tissue p53 in insulin resistance.

Insulin resistance has been reported to correlate with enhanced telomere shortening in young adults[16], whereas aging is known to accelerate telomere dysfunction in various human tissues[1,5]. It is well accepted that dysfunctional (that is, critically short) telomeres resemble damaged DNA and thus trigger a p53-dependent response[17,18]. To investigate a potential relationship between telomere-dependent p53 activation and insulin resistance, we used telomerase reverse transcriptase (*Tert*)-deficient mice. These mice have a normal phenotype in the first generation (G1), presumably because mice possess very long telomeres[19,20]. However, their telomeres become shorter with successive generations, and the mice eventually become infertile by the fourth to sixth generation (G4–G6), owing to impairment of the reproductive system[20]. We fed an HF-HS diet to G4 mice for 8 weeks (from 4 to 12 weeks of age) and examined the effects of cellular aging on glucose metabolism. Although the insulin sensitivity and glucose tolerance of G4 mice were similar to those of wild-type mice on a normal diet, insulin resistance and glucose intolerance became more prominent in G4 mice than in wild-type mice after feeding with the HF-HS diet (**Fig. 3a**). There were no significant differences in weight gain, food intake and oxygen consumption between the two groups (**Fig. 3b**). Expression of proinflammatory cytokines such as *Tnf* and *Ccl2* was increased in the adipose tissue of G4 mice on the HF-HS diet, and this increase was evident in mice with shorter telomeres in adipose cells (**Fig. 3c,d** and **Supplementary Fig. 3a**). Shorter telomeres also promoted the infiltration of macrophages into adipose tissue (**Fig. 3c** and **Supplementary Figs. 2c** and **3b**). Expression of hepatic gluconeogenic enzymes was upregulated in G4 mice (**Fig. 3c**). Insulin-induced phosphorylation of Akt was markedly lower in the liver of G4 mice compared to wild-type mice, and in skeletal muscle to a lesser extent (**Supplementary Fig. 3c**). The adipose tissue of G4 mice on the HF-HS diet showed senescence-like changes, including

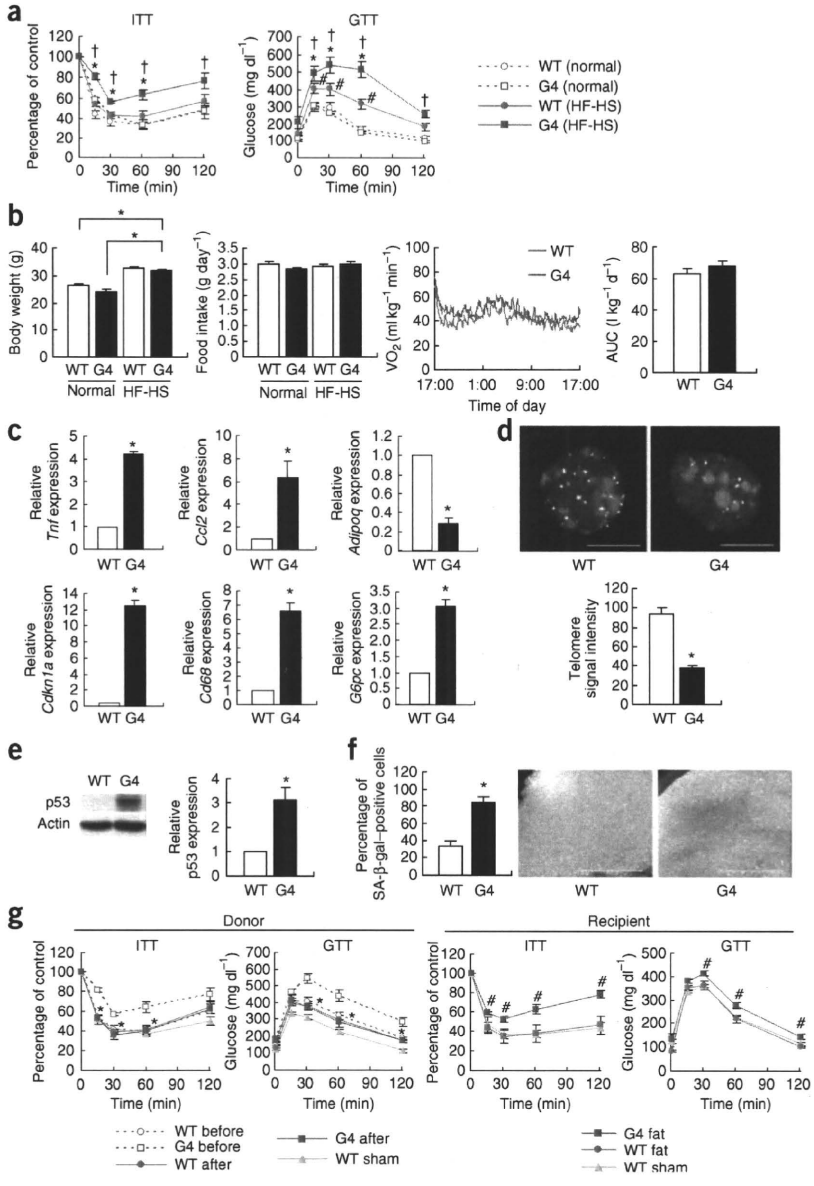

Figure 3 Adipose tissue p53 expression and insulin resistance in G4 mice. (**a**) ITT and GTT after 8 weeks on a HF-HS diet or a normal diet (normal) in G4 and WT mice. $*P < 0.05$ versus WT (HF-HS); $\#P < 0.05$ versus WT (normal); $\dagger P < 0.05$ versus G4 (normal); $n = 7$. (**b**) Body weight, food intake and oxygen consumption (VO_2) in WT and G4 mice. AUC, area under the curve. (**c**) Real-time PCR analysis of the expression of cytokines, *Cdkn1a* and *Cd68* in adipose tissue and the expression of *G6pc* in the livers of WT mice and G4 mice. All mice were fed on the HF-HS diet. (**d**) Top, telomeric fluorescence (yellow) *in situ* hybridization of adipocytes from WT and G4 mice. The signal intensity of the X chromosome (red) was used as an internal control. Bottom, estimation of the length of telomeres in adipose cells by quantification of telomeric fluorescence *in situ* hybridization images. Representative of 30 nuclei (images) for each genotype. Scale bar, 10 μm. (**e**) Expression of p53 in the adipose tissue of WT mice and G4 mice on the HF-HS diet, as determined by western blot analysis. The graph indicates relative expression of p53 protein. (**f**) The number of cells positive for SA-β-gal activity in the adipose tissue of WT mice and G4 mice. Photographs show adipose tissue after SA-β-gal staining. Scale bar, 5 mm. $*P < 0.05$; $n = 6$ for **b**; $n = 5$ for **c**; $n = 30$ nuclei for **d**; $n = 3$ for **e** and **f**. (**g**) Left, ITT and GTT in WT and G4 donor mice before and after fat pad removal. Right, ITT and GTT in recipients of fat pads (1 g) from WT mice (WT fat) or G4 mice (G4 fat) and in sham-operated WT mice (WT sham). $*P < 0.05$ versus G4 before, $\#P < 0.05$ versus WT fat; $n = 6$. Data are shown as the means ± s.e.m.

increased expression of *Cdkn1a* mRNA and p53 protein, as well as enhanced activity of SA-β-gal (**Fig. 3c,e,f** and **Supplementary Fig. 3d**). These results suggest that telomere-dependent senescence of adipose tissue can also promote an inflammatory response, thereby leading to insulin resistance.

To investigate the influence of adipose tissue senescence on the insulin resistance of G4 mice receiving a HF-HS diet, we transplanted epididymal fat pads subcutaneously into wild-type mice and examined the changes of insulin sensitivity and glucose tolerance in the donor and recipient mice. Two weeks after fat pad removal, insulin resistance and glucose intolerance were both markedly improved in G4 mice on the HF-HS diet (**Fig. 3g** and **Supplementary Fig. 2d**). The insulin level of donor G4 mice was also normalized by 2 weeks after fat pad removal (**Supplementary Fig. 3e**). Conversely, implantation of adipose tissue from G4 mice on this diet significantly impaired the insulin sensitivity and glucose tolerance of wild-type recipient mice, whereas implantation of adipose tissue from other wild-type mice fed the same diet had no effect (**Fig. 3g**). Implantation of adipose tissue from G4 mice also lowered insulin-induced phosphorylation of Akt in the liver (**Supplementary Fig. 3f**). Histological examination showed that the implanted adipose tissue was viable and vascularized (**Supplementary Fig. 3g**). Moreover, implantation of fat pads collected from G4 $Trp53^{+/-}$ mice into wild-type mice had less influence on the insulin resistance and glucose tolerance of the recipients (**Supplementary Fig. 3h**) compared with fat pads from G4 $Trp53^{+/+}$ mice. These results indicate that telomere-dependent p53 activation in adipose tissue also leads to insulin resistance.

We noted that expression of histone γ-H2AX, a marker of double-stranded DNA breaks, was increased in the adipose tissue of Ay mice as well as G4 mice (**Fig. 4a**), suggesting a potential role of the ROS-induced DNA damage pathway in the development of type 2 diabetes. To further investigate the relationship between ROS-induced DNA damage and diabetes, we examined the effect of oxidative stress on the expression of inflammatory cytokines in primary cultures of human preadipocytes. Treatment with hydrogen peroxide led to a marked increase of p53 protein expression (**Fig. 4b**). Hydrogen peroxide treatment significantly upregulated expression of *TNF* and *CCL2*, whereas this upregulation was inhibited by p53 knockdown (**Fig. 4c**). This treatment also increased the activity of nuclear factor-κB (NF-κB;

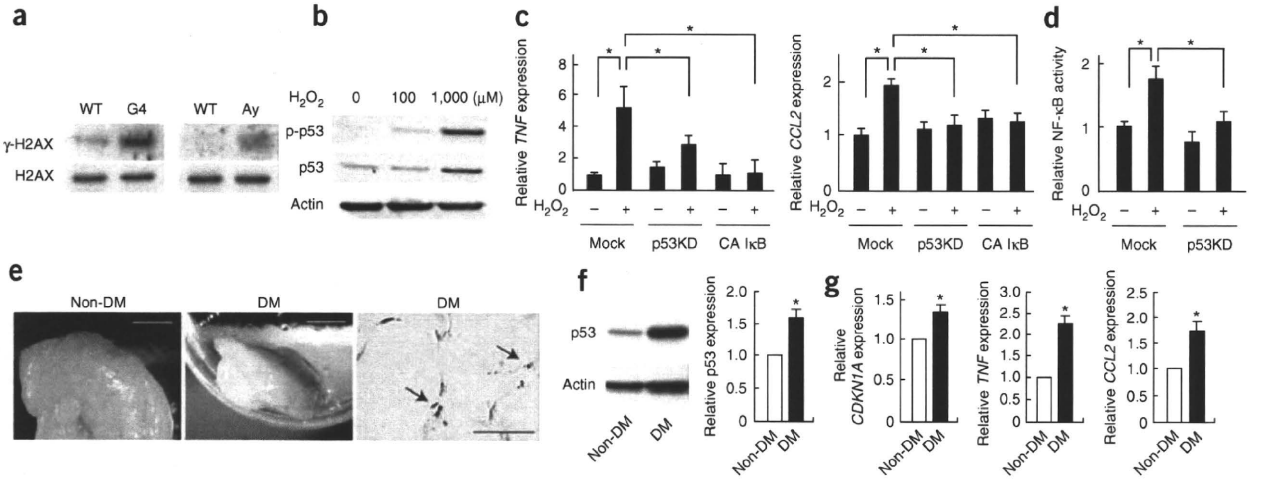

Figure 4 Senescence-like features of adipose tissue from subjects with diabetes. (**a**) Western blot analysis of γ-H2AX expression in adipose tissue of WT mice and G4 mice on a HF-HS diet and WT mice and Ay mice on a normal diet. (**b**) Effect of hydrogen peroxide (H_2O_2) on p53 expression in human preadipocytes by western blot analysis. p-p53, phosphorylated p53. (**c**) Hydrogen peroxide–induced expression of *TNF* and *CCL2* in human preadipocytes transfected with siRNA targeting p53 (p53KD) or the vector encoding constitutively active inhibitor of κB (CA IκB). (**d**) Effect of p53 knockdown (p53KD) on hydrogen peroxide–induced activation of NF-κB. (**e**) Adipose tissue from subjects without diabetes (non-DM) or subjects with diabetes (DM) after SA-β-gal staining. Scale bar, 10 mm. The photograph on the right shows adipose tissue obtained from a subject with diabetes (DM). Arrows indicate SA-β-gal–positive cells. Scale bar, 50 μm. (**f**,**g**) Expression of p53, *CDKN1A* and cytokines in adipose tissue obtained from subjects without diabetes or subjects with diabetes, as determined by western blot analysis (**f**) or real-time PCR (**g**). The graphs indicate relative expression of p53 protein (**f**) and relative mRNA levels of *CDKNA1*, *TNF* and *CCL2* (**g**). $^*P < 0.05$; $n = 5$ for **c**, **d**, **f** and **g**. Data are shown as the means ± s.e.m.

Fig. 4d), a key transcription factor that regulates the induction of cytokines, including *TNF* and *CCL2*, whereas inhibition of NF-κB activation suppressed oxidative stress–induced upregulation of these cytokines (**Fig. 4c**). In agreement with previous reports that induction of p53 causes activation of NF-κB[21,22], we found that p53 deficiency led to a decrease in oxidative stress–induced NF-κB activation (**Fig. 4d**), indicating that ROS-induced p53 activation causes NF-κB–dependent induction of inflammatory cytokines and thus accelerates the development of diabetes.

To determine whether or not senescence-like changes occur in human adipose tissue, we examined visceral fat obtained from subjects undergoing abdominal surgery for primary gastric cancer or colon cancer. Adipose tissue from subjects with diabetes showed increased SA-β-gal activity and higher levels of p53 protein and *CDKN1A* mRNA expression compared with tissue from nondiabetic subjects (**Fig. 4e–g**). Moreover, expression of inflammatory cytokines was significantly increased in diabetic adipose tissue (**Fig. 4g**), suggesting that aging of fat cells has a major role in human diabetes.

Recent studies have shown that longevity signals generated in adipose tissue are crucial in regulating the lifespan of various species, ranging from worms to mice, and suggested that aging is non–cell-autonomously regulated by adipose tissue[23–26]. Consistent with these reports, subcutaneous implantation of senescent adipose tissue from G4 mice accelerates the senescence of epididymal fat in wild-type recipients (T.M., unpublished data). Senescence of adipose tissue may increase the local production of proinflammatory molecules, and it also promotes systemic inflammation and insulin resistance via non–cell-autonomous mechanisms. In contrast, low circulating insulin concentrations are generally associated with longevity, and the activation of longevity signals in adipose tissue has been reported to lower the circulating insulin level and extend the lifespan[27,28]. We found that inhibition of p53 activity in adipose tissue improved insulin resistance and decreased the plasma insulin level. Thus, p53 activation in adipose tissue may be a proaging signal with a negative influence on longevity, whereas inhibition of cellular aging may become a new strategy for the treatment of diabetes as well as aging and its associated diseases.

METHODS

Methods and any associated references are available in the online version of the paper at http://www.nature.com/naturemedicine/.

Note: Supplementary information is available on the Nature Medicine website.

ACKNOWLEDGMENTS

We thank H. Karagiri for discussion, W.C. Greene (University of California) and T. Fujita (The Tokyo Metropolitan Institute of Medical Science) for expression vector encoding constitutively active IκB and p55-A2-Luc (luciferase reporter vector containing the κB binding sites), respectively, A. Berns (The Netherlands Cancer Institute) for floxed *Trp53* mice, and E. Fujita, Y. Ishiyama, R. Kobayashi and Y. Ishikawa for their excellent technical assistance. This work was supported by a Grant-in-Aid for Scientific Research from the Ministry of Education, Science, Sports and Culture and Health and Labor Sciences Research Grants (to I.K.); a Grant-in-Aid for Scientific Research from the Ministry of Education, Culture, Sports, Science and Technology of Japan; and grants from the Suzuken Memorial Foundation, the Japan Diabetes Foundation, the Ichiro Kanehara Foundation, the Tokyo Biochemical Research Foundation, the Takeda Science Foundation, the Cell Science Research Foundation and the Japan Foundation of Applied Enzymology (to T.M.).

AUTHOR CONTRIBUTIONS

T.M. designed and conducted experiments and wrote the manuscript, M.O., I.S., T.K., M.Y., T.I., A. Nojima and Y.O. conducted experiments, A. Nabetani performed telomere analysis, H.M. performed the human studies, F.I. generated telomerase-deficient mice and I.K. evaluated the results, supervised this study and wrote the manuscript.

Published online at http://www.nature.com/naturemedicine/.
Reprints and permissions information is available online at http://npg.nature.com/reprintsandpermissions/.

1. Stewart, S.A. & Weinberg, R.A. Telomeres: cancer to human aging. *Annu. Rev. Cell Dev. Biol.* **22**, 531–557 (2006).
2. Serrano, M. & Blasco, M.A. Putting the stress on senescence. *Curr. Opin. Cell Biol.* **13**, 748–753 (2001).
3. Campisi, J. Senescent cells, tumor suppression, and organismal aging: good citizens, bad neighbors. *Cell* **120**, 513–522 (2005).

4. Shay, J.W. & Wright, W.E. Senescence and immortalization: role of telomeres and telomerase. *Carcinogenesis* **26**, 867–874 (2005).
5. Minamino, T. & Komuro, I. Vascular cell senescence: contribution to atherosclerosis. *Circ. Res.* **100**, 15–26 (2007).
6. Minamino, T. & Komuro, I. Vascular aging: insights from studies on cellular senescence, stem cell aging, and progeroid syndromes. *Nat. Clin. Pract. Cardiovasc. Med.* **5**, 637–648 (2008).
7. Greider, C.W. Telomere length regulation. *Annu. Rev. Biochem.* **65**, 337–365 (1996).
8. Herbig, U., Ferreira, M., Condel, L., Carey, D. & Sedivy, J.M. Cellular senescence in aging primates. *Science* **311**, 1257 (2006).
9. Dimri, G.P. *et al.* A biomarker that identifies senescent human cells in culture and in aging skin in vivo. *Proc. Natl. Acad. Sci. USA* **92**, 9363–9367 (1995).
10. Furukawa, S. *et al.* Increased oxidative stress in obesity and its impact on metabolic syndrome. *J. Clin. Invest.* **114**, 1752–1761 (2004).
11. Hotamisligil, G.S., Shargill, N.S. & Spiegelman, B.M. Adipose expression of tumor necrosis factor-α: direct role in obesity-linked insulin resistance. *Science* **259**, 87–91 (1993).
12. Weisberg, S.P. *et al.* Obesity is associated with macrophage accumulation in adipose tissue. *J. Clin. Invest.* **112**, 1796–1808 (2003).
13. Kamei, N. *et al.* Overexpression of monocyte chemoattractant protein-1 in adipose tissues causes macrophage recruitment and insulin resistance. *J. Biol. Chem.* **281**, 26602–26614 (2006).
14. Makowski, L. *et al.* Lack of macrophage fatty-acid–binding protein aP2 protects mice deficient in apolipoprotein E against atherosclerosis. *Nat. Med.* **7**, 699–705 (2001).
15. Makowski, L., Brittingham, K.C., Reynolds, J.M., Suttles, J. & Hotamisligil, G.S. The fatty acid–binding protein, aP2, coordinates macrophage cholesterol trafficking and inflammatory activity. Macrophage expression of aP2 impacts peroxisome proliferator–activated receptor γ and IκB kinase activities. *J. Biol. Chem.* **280**, 12888–12895 (2005).
16. Gardner, J.P. *et al.* Rise in insulin resistance is associated with escalated telomere attrition. *Circulation* **111**, 2171–2177 (2005).
17. Chin, L. *et al.* p53 deficiency rescues the adverse effects of telomere loss and cooperates with telomere dysfunction to accelerate carcinogenesis. *Cell* **97**, 527–538 (1999).
18. Karlseder, J., Broccoli, D., Dai, Y., Hardy, S. & de Lange, T. p53- and ATM-dependent apoptosis induced by telomeres lacking TRF2. *Science* **283**, 1321–1325 (1999).
19. Blasco, M.A. *et al.* Telomere shortening and tumor formation by mouse cells lacking telomerase RNA. *Cell* **91**, 25–34 (1997).
20. Lee, H.W. *et al.* Essential role of mouse telomerase in highly proliferative organs. *Nature* **392**, 569–574 (1998).
21. Ryan, K.M., Ernst, M.K., Rice, N.R. & Vousden, K.H. Role of NF-κB in p53-mediated programmed cell death. *Nature* **404**, 892–897 (2000).
22. Benoit, V. *et al.* Transcriptional activation of cyclooxygenase-2 by tumor suppressor p53 requires nuclear factor-κB. *Oncogene* **25**, 5708–5718 (2006).
23. Kenyon, C. The plasticity of aging: insights from long-lived mutants. *Cell* **120**, 449–460 (2005).
24. Hwangbo, D.S., Gershman, B., Tu, M.P., Palmer, M. & Tatar, M. *Drosophila* dFOXO controls lifespan and regulates insulin signalling in brain and fat body. *Nature* **429**, 562–566 (2004).
25. Giannakou, M.E. *et al.* Long-lived *Drosophila* with overexpressed dFOXO in adult fat body. *Science* **305**, 361 (2004).
26. Blüher, M., Kahn, B.B. & Kahn, C.R. Extended longevity in mice lacking the insulin receptor in adipose tissue. *Science* **299**, 572–574 (2003).
27. Blüher, M. *et al.* Adipose tissue selective insulin receptor knockout protects against obesity and obesity-related glucose intolerance. *Dev. Cell* **3**, 25–38 (2002).
28. Libina, N., Berman, J.R. & Kenyon, C. Tissue-specific activities of *C. elegans* DAF-16 in the regulation of lifespan. *Cell* **115**, 489–502 (2003).

ONLINE METHODS

Animal models. The study protocol was approved by the Chiba University Institutional Animal Care and Use Committee. The creation of mice deficient in *Tert* has been described previously[29]. We backcrossed heterozygous mice with wild-type C57BL/6 mice (SLC) for six generations and intercrossed them to produce G1 $Tert^{-/-}$ mice. Mating of G1 $Tert^{-/-}$ mice with each other generated G2 mice, after which we produced $Tert^{-/-}$ mice up to the fourth generation (G4). We purchased p53-deficient mice (with a C57BL/6 background) from Jackson Laboratories and mated them with $Tert^{+/-}$ mice to generate double heterozygotes ($Tert^{+/-}$ $Trp53^{+/-}$). We intercrossed these mice to generate G1 $Tert^{-/-}$ $Trp53^{+/-}$ mice. We mated G1 $Tert^{-/-}$ $Trp53^{+/-}$ mice with other G1 mice to produce G2 $Tert^{-/-}$ $Trp53^{+/-}$ mice, after which we repeated this mating strategy to generate G4 $Tert^{-/-}$ $Trp53^{+/-}$ mice. We fed the mice a HF-HS diet (Oriental Yeast)[30] or normal chow from 4 to 12 weeks of age before we performed metabolic analyses. We purchased Ay mice (with a C57BL/6 background) from Jackson Laboratories and mated them with $Trp53^{+/-}$ mice to generate $Trp53^{+/+}$, Ay $Trp53^{+/+}$, $Trp53^{+/-}$ and Ay $Trp53^{+/-}$ mice. We fed these mice normal chow and analyzed them at 20 weeks of age. We purchased mice that express Cre recombinase in adipocytes (Fabp4-Cre) from Jackson Laboratories. We then crossed Fabp4-Cre mice (with a C57BL/6 background) with mice that carry floxed *Trp53* alleles (with a C57BL/6 background)[31] to generate adipocyte-specific p53-knockout mice. We fed these mice a HF-HS diet or normal chow for 4 months before we performed metabolic analyses. Littermate controls had the genotype $Cre^{-}Trp53^{loxP/-}$ or $Cre^{-}Trp53^{loxP/loxP}$. We also generated transgenic mice (with a C57BL/6 background) that carry the *loxP-LacZ-loxP* cassette flanked by the *TP53* complementary DNA fragment under the control of the cytomegalovirus enhancer–chicken actin promoter. Expression of transgene-derived *TP53* was prevented by the *loxP-LacZ-loxP* cassette. When we bred these transgenic mice with Fabp4-Cre mice, the floxed *LacZ* cassette was excised in the resulting offspring ($Cre^{+}LacZ\text{-}TP53^{+}$), and we observed upregulation of p53 expression in adipose tissue (adipo-p53–transgenic mice). We fed these mice normal chow and analyzed them at 10–12 weeks of age. Littermate controls had the genotype $Cre^{-}LacZ\text{-}TP53^{+}$.

Cell culture. We purchased human preadipocytes from Sanko, and we cultured them according to the manufacturer's instructions.

Western blot analysis. We resolved whole-cell lysates (30–50 μg) by SDS PAGE. We transferred the proteins onto a polyvinylidene difluoride (PVDF) membrane (Millipore) incubated them with the primary antibody (**Supplementary Methods**), followed by incubation with rabbit IgG–specific horseradish peroxidase–conjugated antibody (111-035-003) or mouse IgG–specific horseradish peroxidase–conjugated antibody (115-035-003; Jackson). We detected specific proteins by enhanced chemiluminescence (Amersham).

Human subjects. The ethical committee of Chiba University Graduate School of Medicine reviewed and approved the study protocol. We enrolled 10 subjects (56–68 years old; six males and four females) who were admitted to Chiba University Hospital and underwent surgery for primary gastric or colon cancer. We obtained informed consent from all subjects before inclusion in the study.

Statistical analyses. Data are shown as the means ± s.e.m. We examined differences between groups by Student's *t* test or analysis of variance followed by Bonferroni's correction for comparison of means. For all analyses, we considered $P < 0.05$ as statistically significant.

Additional methods. Detailed methodology is described in the **Supplementary Methods**.

29. Yuan, X. *et al.* Presence of telomeric G-strand tails in the telomerase catalytic subunit TERT knockout mice. *Genes Cells* **4**, 563–572 (1999).
30. Maeda, N. *et al.* Diet-induced insulin resistance in mice lacking adiponectin/ACRP30. *Nat. Med.* **8**, 731–737 (2002).
31. Marino, S., Vooijs, M., van Der Gulden, H., Jonkers, J. & Berns, A. Induction of medulloblastomas in p53-null mutant mice by somatic inactivation of Rb in the external granular layer cells of the cerebellum. *Genes Dev.* **14**, 994–1004 (2000).

Journal of Molecular and Cellular Cardiology 47 (2009) 664–675

Contents lists available at ScienceDirect

Journal of Molecular and Cellular Cardiology

journal homepage: www.elsevier.com/locate/yjmcc

Original article

Interaction of myocardial insulin receptor and IGF receptor signaling in exercise-induced cardiac hypertrophy

Hiroyuki Ikeda [a,b], Ichiro Shiojima [a,c], Yukako Ozasa [a], Masashi Yoshida [a], Martin Holzenberger [d], C. Ronald Kahn [e], Kenneth Walsh [f], Takashi Igarashi [b], E. Dale Abel [g], Issei Komuro [a,c,*]

[a] Department of Cardiovascular Science and Medicine, Chiba University Graduate School of Medicine, Chiba, Japan
[b] Department of Pediatrics, University of Tokyo Graduate School of Medicine, Tokyo, Japan
[c] Department of Cardiovascular Medicine, Osaka University Graduate School of Medicine, Suita, Japan
[d] INSERM UMR893, Saint-Antoine Hospital, Paris, France
[e] Joslin Diabetes Center and Department of Medicine, Harvard Medical School, Boston, MA, USA
[f] Molecular Cardiology, Whitaker Cardiovascular Institute, Boston University School of Medicine, Boston, MA, USA
[g] Program in Molecular Medicine and Division of Endocrinology, Metabolism, and Diabetes, University of Utah School of Medicine, Salt Lake City, UT, USA

ARTICLE INFO

Article history:
Received 14 April 2009
Received in revised form 9 August 2009
Accepted 25 August 2009
Available online 8 September 2009

Keywords:
Insulin-like growth factor receptor
Insulin receptor
Exercise
Cardiac hypertrophy
Tyrosine phosphorylation

ABSTRACT

Insulin-like growth factor-1 (IGF-1) signaling has recently been implicated in the development of cardiac hypertrophy after long-term endurance training, via mechanisms that may involve energetic stress. Given the potential overlap of insulin and IGF-1 signaling we sought to determine if both signaling pathways could contribute to exercise-induced cardiac hypertrophy following shorter-term exercise training. Studies were performed in mice with cardiac-specific IGF-1 receptor (IGF1R) knockout (CIGFRKO), mice with cardiac-specific insulin receptor (IR) knockout (CIRKO), CIGFRKO mice that lacked one IR allele in cardiomyocytes (IGFR−/−IR+/−), and CIRKO mice that lacked one IGF1R allele in cardiomyocytes (IGFR+/−IR−/−). Intravenous administration of IGF-1 or 75 hours of swimming over 4 weeks increased IGF1R tyrosine phosphorylation in the heart in control and CIRKO mice but not in CIGFRKO mice. Intriguingly, IR tyrosine phosphorylation in the heart was also increased following IGF-1 administration or exercise training in control and CIGFRKO mice but not in CIRKO mice. The extent of cardiac hypertrophy following exercise training in CIGFRKO and CIRKO mice was comparable to that in control mice. In contrast, exercise-induced cardiac hypertrophy was significantly attenuated in IGFR−/−IR+/− and IGFR+/−IR−/− mice. Thus, IGF-1 and exercise activates both IGF1R and IR in the heart, and IGF1R- and IR-mediated signals may serve redundant roles in the hypertrophic responses of the heart to exercise training.

1. Introduction

Postnatal myocardial growth is primarily achieved through hypertrophy of individual myocytes [1]. In addition to normal heart growth during postnatal development, heart size increases in response to various forms of both extrinsic and intrinsic stimuli [2], and these hypertrophic responses are classified either as "pathological" or "physiological." Pathological cardiac hypertrophy is frequently associated with contractile dysfunction and histological pathology such as interstitial fibrosis, and is typically observed in patients with hypertension, myocardial infarction, and valvular heart diseases. On the other hand, physiological cardiac hypertrophy is characterized by normal or enhanced contractility and normal cardiac architecture, as typically observed in trained athletes [3,4]. Notably, exercise training is beneficial in a selected population of heart failure patients [5] and reverses molecular and functional abnormalities of the heart in animal models of pathological hypertrophy [6–8]. Thus, promoting physiological cardiac hypertrophy may be one of the therapeutic options for heart diseases.

The insulin-like growth factor-1 (IGF-1)–phosphatidylinositol 3-kinase (PI3K)–Akt pathway has been implicated in the development of exercise-induced cardiac hypertrophy [9,10]. Increased cardiac IGF-1 formation is associated with physiological hypertrophy in athletes [11], and exercise training increases IGF-1 mRNA expression in rat hearts [12]. Overexpression of IGF-1 in the heart in transgenic mice induces physiological cardiac hypertrophy in the early phases of postnatal development [13], and IGF-1 receptor (IGF1R) overexpression in the heart results in physiological cardiac hypertrophy associated with activation of the PI3K-Akt pathway [14]. Overexpression of a constitutively active p110α PI3K results in physiological cardiac hypertrophy [15], and exercise-induced hypertrophy is completely abolished by dominant-negative p110α overexpression [14,16]. Short-term or moderate levels of Akt1 overexpression in the heart induces physiological cardiac hypertrophy [17,18], whereas development of exercise-induced cardiac hypertrophy is blunted in Akt1 knockout mice [19].

* Corresponding author. Department of Cardiovascular Science and Medicine, Chiba University Graduate School of Medicine, Chiba, Japan.
E-mail address: komuro-tky@umin.ac.jp (I. Komuro).

0022-2828/$ – see front matter © 2009 Elsevier Inc. All rights reserved.
doi:10.1016/j.yjmcc.2009.08.028

These results collectively suggest that IGF-1 or IGF1R is sufficient whereas PI3K–Akt pathway is both necessary and sufficient to induce physiological cardiac hypertrophy. A recent study in mice with cardiomyocyte-restricted deletion of IGF1R suggested that cardiac IGF1R signaling could modulate exercise-induced cardiac hypertrophy [20]. In this study, 96 hours of swim training over 5 weeks led to increased AMPK activation in IGF1R-deficient hearts, and AMPK activation was postulated to have a negative impact on cardiac hypertrophy. Insulin receptor (IR)-mediated signals have also been implicated in the regulation of cardiac growth and function. Cardiac-specific IR knockout (CIRKO) mice exhibit small heart size with mildly impaired contractility and reduced Akt activity [21,22], suggesting that IR-mediated signals could potentially play a role in exercise-induced physiological hypertrophy.

To elucidate the role of IGF1R and IR in the development of exercise-induced cardiac hypertrophy, we subjected cardiac-specific IGF1R knockout (CIGFRKO) mice and CIRKO mice to 75 hours of swimming over 4 weeks. Although both CIGFRKO mice and CIRKO mice developed exercise-induced cardiac hypertrophy to the level comparable to their wild type littermates, deletion of a single *Ir* or a single *Igf1r* allele on CIGFRKO or CIRKO background, respectively, blunted hypertrophic responses to exercise. We also observed that tyrosine phosphorylation of both IGF1R and IR was increased in the heart after intravenous IGF-1 administration or exercise training. Thus, IGF-1 and exercise may activate both IGF1R and IR in the heart, and IGF1R- and IR-mediated signals may play redundant roles in the development of cardiac hypertrophy in response to exercise training.

2. Materials and methods

2.1. Animals, exercise training, and IGF-1 administration

CIGFRKO mice were initially generated by crossing $Igf1r^{flox/flox}$ mice [23] with α-myosin heavy chain (αMHC)-Cre transgenic mice [24]. Subsequent maintenance of CIGFRKO line was done by crossing CIGFRKO mice ($Igf1r^{flox/flox}Cre^{+/-}$) with $Igf1r^{flox/flox}Cre^{-/-}$ mice. CIRKO mice were generated as described previously [21]. Subsequent maintenance of CIRKO line was done by crossing CIRKO mice ($Ir^{flox/flox}Cre^{+/-}$) with $Ir^{flox/flox}Cre^{-/-}$ mice. Cardiac-specific *Igf1r*−/−*Ir*+/− mice and *Igf1r*+/−*Ir*−/− mice were generated by crossing $Igf1r^{flox/flox}Ir^{flox/flox}Cre^{-/-}$ mice with CIGFRKO mice ($Igf1r^{flox/flox}Ir^{+/+}Cre^{+/-}$) and CIRKO mice ($Igf1r^{+/+}Ir^{flox/flox}Cre^{+/-}$), respectively. Animals were on a mixed background of C57BL/6J, 129Sv, and FVB, and littermates that contain the same combination of *Igf1r*/*Ir* alleles but do not contain αMHC-Cre transgene were used as wild type controls in each study (Supplementary Fig. S1). Genotyping was performed as described [21,25].

Swimming training was performed in 10-week-old male mice as described previously [26]. Swimming sessions were done twice a day for 28 days. The first 7 days consisted of a training period in which one session was 20 min long on the first day and it was increased by 10 min per day. On the subsequent 21 days, two sessions of 90 min swimming were done. After the final swimming session, mice were overnight fasted and sacrificed. M-mode tracings of left ventricular wall motion at the level of papillary muscle were obtained using Vevo 660 Imaging system (Visual Sonic) with a 25-MHz transducer. For IGF-1 or insulin administration, mice were overnight fasted and anesthetized with pentobarbital, and IGF-1 (Fujisawa Co., Japan) or insulin (Lilly Co., Japan) was intravenously administered. Animals were sacrificed 5 minutes after IGF-1 or insulin administration. All animal procedures were performed with the approval of the Institutional Animal Care and Use Committee of Chiba University.

2.2. Histological analysis

Hearts were fixed and embedded in paraffin for histological analyses. Serial sections of 4 μm were stained with hematoxylin and eosin (HE) for morphological analysis and Masson's trichrome (MT) for detection of fibrosis. For measurements of myocyte cross-sectional area, immunohistochemistry with anti-dystrophin antibody (Novocastra Laboratories, Newcastle, UK) was performed to visualize myocyte membranes. The sections were reacted with anti-dystrophin

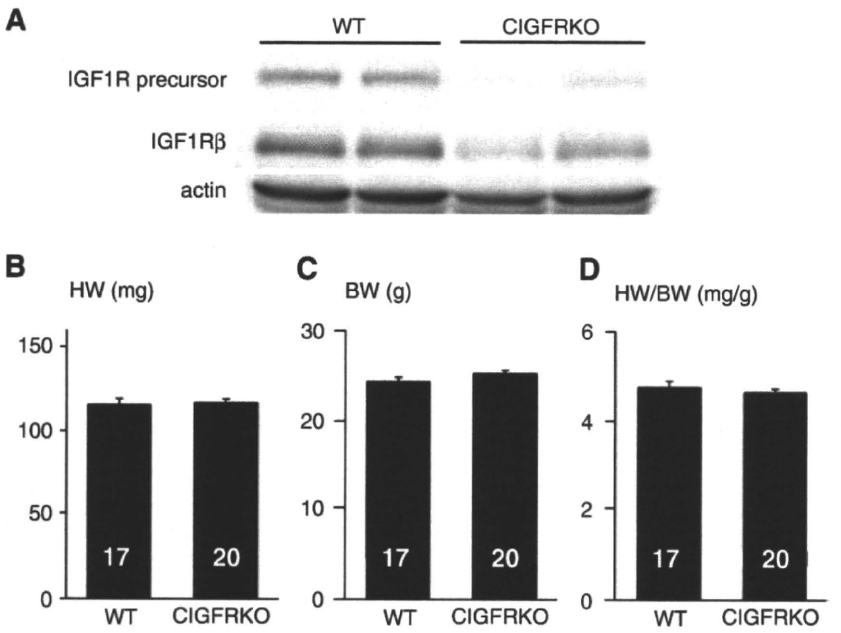

Fig. 1. CIGFRKO mice exhibit no obvious cardiac phenotype at baseline. (A) Expression of IGF1R precursor protein and IGF1R β subunit protein (IGF1Rβ) as revealed by Western blot analysis of whole heart lysates. Actin served as internal control. (B–D) HW (B), BW (C), and HW/BW ratio (D) of WT and CIGFRKO mice at 10 weeks of age. The number of mice analyzed is shown in the bar.

antibody at 1:20 and visualized by ABC method. Suitable cross-sections for measurements were defined as having round-to-oval membrane staining using ImageJ software. At least 200 myocytes were measured in each sample.

2.3. Western blot analysis and immunoprecipitation

Total protein lysate was extracted from heart tissue and SDS–PAGE was performed as described previously [22]. Anti-IGF1Rβ, anti-IRβ, and anti-phosphotyrosine (PY20) antibodies were from Santa Cruz Biotechnology (Santa Cruz, CA), and anti-actin antibody was from Sigma (St. Louis, MO). For immunoprecipitation, total heart lysates (500 μg protein) were precleared with protein G-agarose beads for an hour before incubation with the indicated antibody (1 μg) overnight at 4 °C. Protein G-agarose beads were added for 3 hours and immunoprecipitates were washed three times in lysis buffer, eluted in 2×SDS buffer and subjected to SDS–PAGE.

2.4. Statistical analysis

Data are shown as mean ± SEM. Statistical significance was determined by Student's t test or Welch's test. P values of <0.05 were considered to be statistically significant.

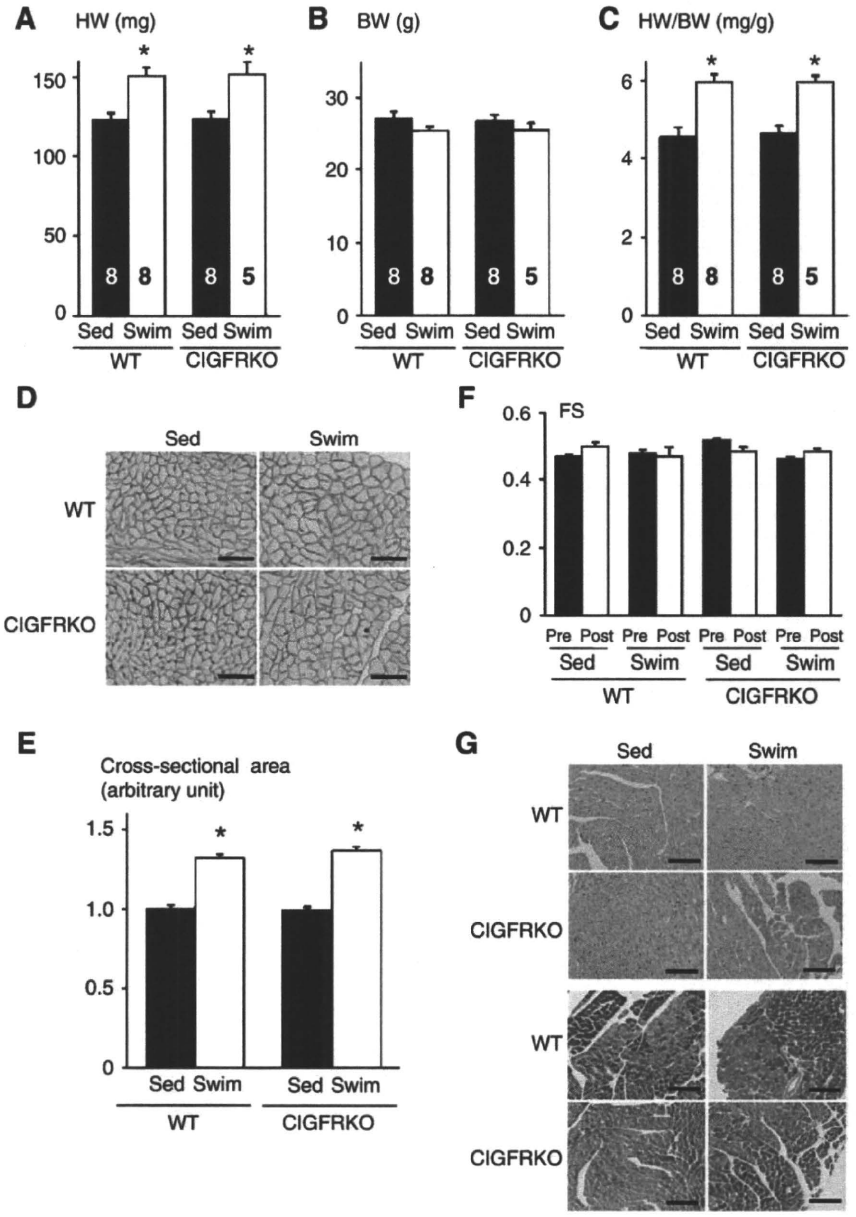

Fig. 2. CIGFRKO mice develop physiological cardiac hypertrophy in response to exercise training. (A–C) HW (A), BW (B), and HW/BW ratio (C) of WT and CIGFRKO mice. *$p<0.05$ versus Sed group of the same genotype. The number of mice analyzed is shown in the bar. (D) Immunohistochemistry with anti-dystrophin antibody. Scale bar = 50 μm. (E) Myocyte cross-sectional area of WT and CIGFRKO mice. *$p<0.05$ versus Sed group of the same genotype. (F) Left ventricular contractile function as assessed by echocardiographic measurement of fractional shortening (FS). Pre and Post represent before and after exercise, respectively. (G) Histological analysis with HE (upper panel) and Masson's trichrome (MT) (lower panel) staining. Scale bar = 100 μm. Sed and Swim represent a sedentary and a swimming group, respectively.

3. Results

3.1. CIGFRKO mice exhibit no cardiac phenotype at baseline

CIGFRKO mice were initially generated by crossing *Igf1r*$^{flox/flox}$ animals with αMHC-Cre transgenic mice, and compared with wild type controls. Western blot analysis of heart lysate revealed that the expression levels of IGF1R precursor protein and IGF1R β subunit protein were reduced, and small amount of proteins detected by western blots were considered to be derived from non-myocytes in the heart (Fig. 1A). At 10 weeks of age, there was no significant difference in heart weight (HW), body weight (BW), heart weight (HW)/BW ratio, and cardiac function as assessed by echocardiography between CIGFRKO mice and wild type (WT) littermates (Figs. 1B–D, and data not shown). Similar results were obtained in other ages. Thus, CIGFRKO mice exhibit no obvious cardiac phenotype at baseline.

3.2. Deletion of *Igf1r* in cardiac myocytes does not attenuate exercise-induced physiological cardiac hypertrophy

Lack of obvious cardiac phenotype in CIGFRKO mice at baseline prompted us to investigate the effect of *Igf1r* deletion on hypertrophic responses of the heart to exercise training. After 75 hours of swimming over 4 weeks, WT and CIGFRKO mice developed similar degrees of cardiac hypertrophy as measured by HW and HW/BW ratio (Figs. 2A-C). The fold increase in myocyte cross-sectional area was also comparable between WT and CIGFRKO animals (Figs. 2D and E). Left ventricular contractile function as measured by echocardiography did not differ between WT and CIGFRKO mice (Fig. 2F), and histological analyses revealed that there was no interstitial fibrosis or myocyte disarray in the hearts of WT and CIGFRKO mice (Fig. 2G). The presence of Cre recombinase in the heart did not affect the extent of hypertrophy or contractile function following exercise training (Supplementary Fig. S2). These results collectively suggest that exercise-induced physiological cardiac hypertrophy may develop normally in the absence of IGF1R-mediated signals in cardiac myocytes.

3.3. IR is phosphorylated by IGF-I in the hearts of WT and CIGFRKO mice

Since IGF-1 signaling has been implicated in the development of physiological cardiac hypertrophy, the above-mentioned results were somewhat unexpected. We first examined whether IGF1R-mediated signals were disrupted in cardiac myocytes of CIGFRKO mice. Western blot analysis of whole heart extracts revealed that, although IGF1R protein levels were upregulated after exercise training in the hearts of WT mice, the expression levels of IGF1R remained at low levels both in sedentary and swim-trained CIGFRKO hearts (Fig. 3A). Tyrosine phosphorylation levels of IGF1R and IR were also examined in the heart of WT and CIGFRKO mice after exercise training. Exercise training increased phosphorylation levels of both IGF1R and IR in the heart of WT mice. Increased phosphorylation levels of IGF1R could be in part attributed to upregulation of IGF1R protein levels following exercise training. As expected, IGF1R phosphorylation but not IR phosphorylation was blunted in the heart of CIGFRKO animals (Fig. 3B). IGF1R tyrosine phosphorylation levels were also examined in the hearts of WT and CIGFRKO mice after intravenous IGF-1 administration. Phosphotyrosine blot after IGF1R immunoprecipitation

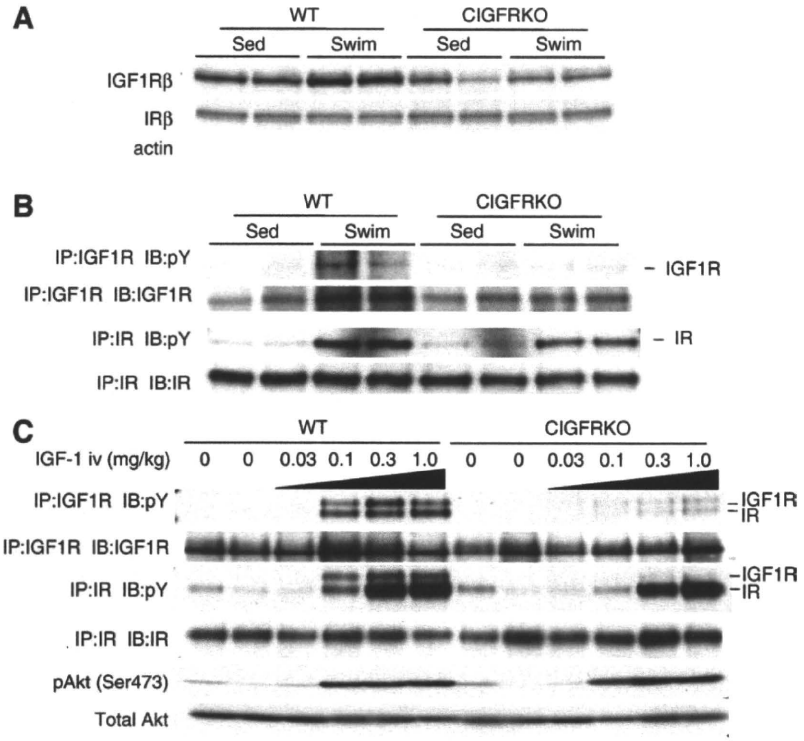

Fig. 3. Western blot analysis of CIGFRKO heart extracts after exercise or IGF-I administration. (A) Expression of IGF1R β subunit protein (IGF1Rβ) and IR β subunit protein (IRβ) in the heart of WT and CIGFRKO mice. Sed and Swim represent a sedentary and a swimming group, respectively. (B) Tyrosine phosphorylation levels of IGF1R and IR following exercise training. pY represents anti-phosphotyrosine antibody. IP and IB represent immunoprecipitation and immunoblot, respectively. (C) Tyrosine phosphorylation levels of IGF1R/IR and activation of Akt in the heart of WT and CIGFRKO mice 5 minutes after IGF-1 administration. There are some IGF1R bands in the immunoprecipitates of IR and vice versa, possibly due to antibody cross-reactivity. pY represents anti-phosphotyrosine antibody. IP and IB represent immunoprecipitation and immunoblot, respectively.

revealed that tyrosine phosphorylation of IGF1R was markedly reduced in CIGFRKO hearts when compared to that of WT hearts (Fig. 3C, upper panel). These findings strongly suggest that IGF1R-mediated signaling is functionally disrupted in cardiac myocytes of CIGFRKO animals. In the same experimental condition, phosphotyrosine blot after IR immunoprecipitation revealed significant tyrosine phosphorylation of IR both in WT and CIGFRKO hearts after IGF-1 administration (Fig. 3C, middle panel), and phospho-Akt levels in the heart were comparable between WT and CIGFRKO animals (Fig. 3C, lower panel). These observations collectively suggest that IR activated by IGF-1 in part mediates exercise-induced physiological cardiac hypertrophy and that IR compensates for the loss of IGF1R-mediated signaling in the hearts of CIGFRKO mice following exercise training.

3.4. Deletion of Ir in cardiac myocytes does not attenuate exercise-induced physiological cardiac hypertrophy

To test the hypothesis that IR mediates exercise-induced physiological cardiac hypertrophy, CIRKO mice and wild type littermates were subjected to exercise training. After 75 hours of swimming, WT and CIRKO mice exhibited similar degrees of cardiac hypertrophy as

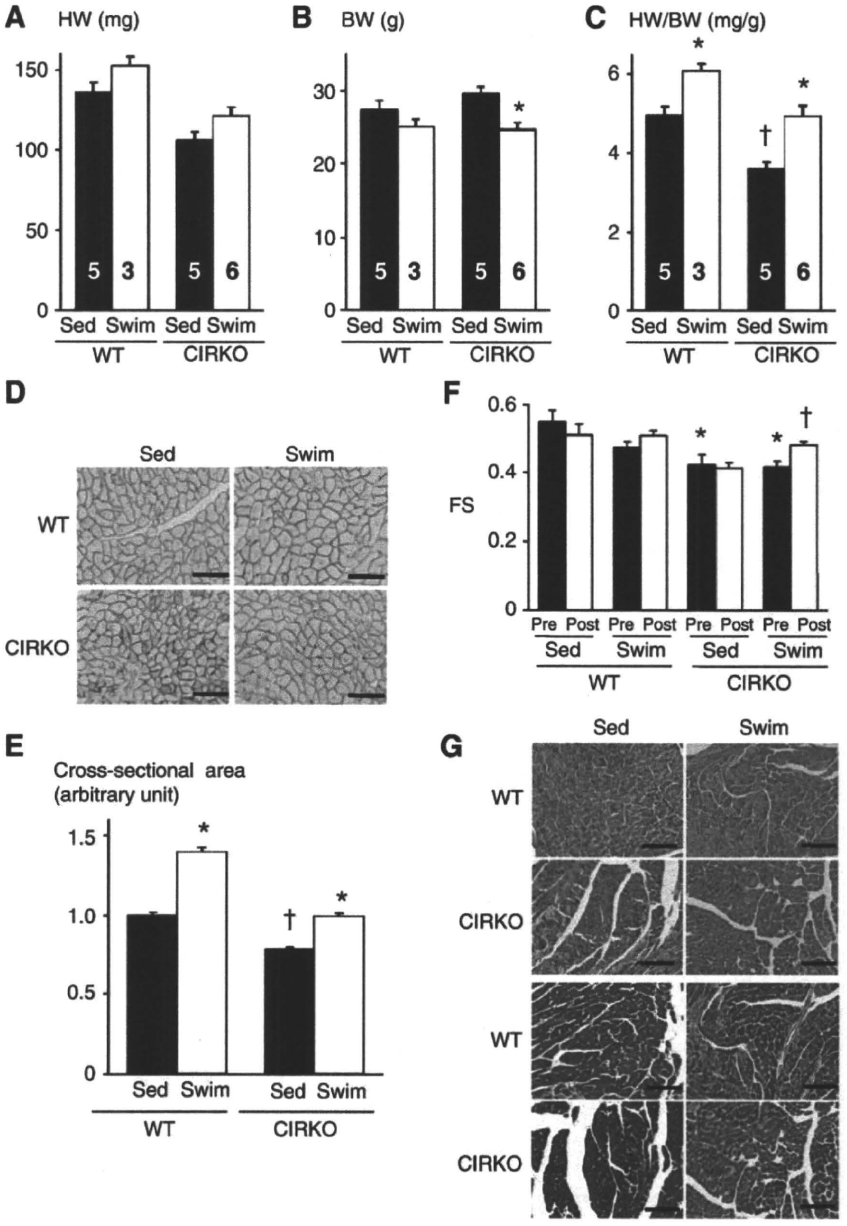

Fig. 4. CIRKO mice develop physiological cardiac hypertrophy in response to exercise training. (A–C) HW (A), BW (B), and HW/BW ratio (C) of WT and CIRKO mice. *p<0.05 versus Sed group of the same genotype, †p<0.05 versus WT Sed group. The number of mice analyzed is shown in the bar. (D) Immunohistochemistry with anti-dystrophin antibody. Scale bar = 50 μm. (E) Myocyte cross-sectional area of WT and CIRKO mice. *p<0.05 versus Sed group of the same genotype. †p<0.05 versus WT Sed group. (F) Left ventricular contractile function as assessed by echocardiographic measurement of fractional shortening (FS). Pre and Post represent before and after exercise, respectively. *p<0.05 versus WT Sed Pre group, †p<0.05 versus CIRKO Swim Pre group. (G) Histological analysis with HE (upper panel) and Masson's trichrome (MT) (lower panel) staining. Scale bar = 100 μm. Sed and Swim represent a sedentary and a swimming group, respectively.

measured by HW (12% versus 14%) and HW/BW ratio (22% versus 38%) (Figs. 4A–C). The fold increase in myocyte cross-sectional area was also significant in WT and CIGFRKO animals (40% and 27%, respectively) (Figs. 4D and E). The relatively enhanced response in HW/BW ratio following exercise was considered to be due to a significant decrease in BW in CIRKO mice following exercise training (Fig. 4B). Interestingly, left ventricular contractile function as assessed by fractional shortening was slightly impaired in CIRKO mice, which was ameliorated by exercise training (Fig. 4F). There was no sign of pathology in histological examination both in WT or CIRKO hearts (Fig. 4G). Thus, exercise-induced physiological cardiac hypertrophy develops normally even in the absence of IR-mediated signals in cardiac myocytes.

Western blot analysis of whole heart extracts revealed that the expression levels of IGF1R were increased in CIRKO hearts at the sedentary state compared to those of WT hearts, and further upregulated after exercise both in WT and CIRKO hearts (Fig. 5A). Tyrosine phosphorylation levels of IGF1R were upregulated both in WT and CIRKO hearts after exercise training, whereas those of IR were upregulated in WT hearts but not in CIRKO hearts (Fig. 5B). When IGF-1 was intravenously administered, phosphotyrosine blot after IGF1R immunoprecipitation revealed that tyrosine phosphorylation of IGF1R was comparable between CIRKO hearts and WT hearts (Fig. 5C, upper panel), whereas phosphotyrosine blot after IR immunoprecipitation revealed that IR tyrosine phosphorylation by IGF-I was markedly reduced in CIRKO hearts (Fig. 5C, middle panel). Phospho-Akt levels in the heart were comparable between WT and CIRKO animals (Fig. 5C, lower panel). These observations indicate that IR-mediated signals are dispensable for the development of exercise-induced physiological cardiac hypertrophy.

3.5. Combined deletion of *Igf1r* and *Ir* attenuates exercise-induced physiological cardiac hypertrophy

The observation that the deletion of either *Igf1r* alone or *Ir* alone in cardiac myocytes does not attenuate swimming-induced cardiac hypertrophy suggests that IGF1R- and IR-mediated signals could compensate for each other during the development of exercise-induced physiological cardiac growth. To test this hypothesis, we generated compound mutants of *Igf1r* and *Ir* genes in the heart. Homozygous deletion of both genes in cardiac myocytes resulted in severe heart failure and early postnatal lethality (data not shown), consistent with a previous report in which *Igf1r* and *Ir* genes were disrupted in cardiac and skeletal muscle cells [27]. We therefore analyzed mice lacking two *Igf1r* alleles and one *Ir* allele (IGF1R−/−IR+/−) or mice lacking one *Igf1r* allele and two *Ir* alleles (IGF1R+/−IR−/−) in cardiac myocytes.

At sedentary state, HW and HW/BW ratio of IGF1R−/−IR+/− mice was comparable to that of WT mice. When these animals were subjected to 75 hours of swimming, the increase in HW and HW/BW ratio was significantly reduced in IGF1R−/−IR+/− mice compared to WT mice (Figs. 6A–C). The increase in myocyte cross-sectional area was also significantly reduced in IGF1R−/−IR+/− animals compared to WT littermates (Figs. 6D and E). Left ventricular contractile function was not affected by gene deletion and/or exercise training (Fig. 6F), and there was no pathological finding on histology (Fig. 6G). Western blot analysis of whole heart extracts revealed that the expression levels of IR were slightly reduced in IGF1R−/−IR+/− hearts and were not altered by exercise (Fig. 7A). When IGF-1 was intravenously administered, tyrosine phosphorylation of IGF1R was markedly reduced (Fig. 7B, upper panel) and that of IR was also

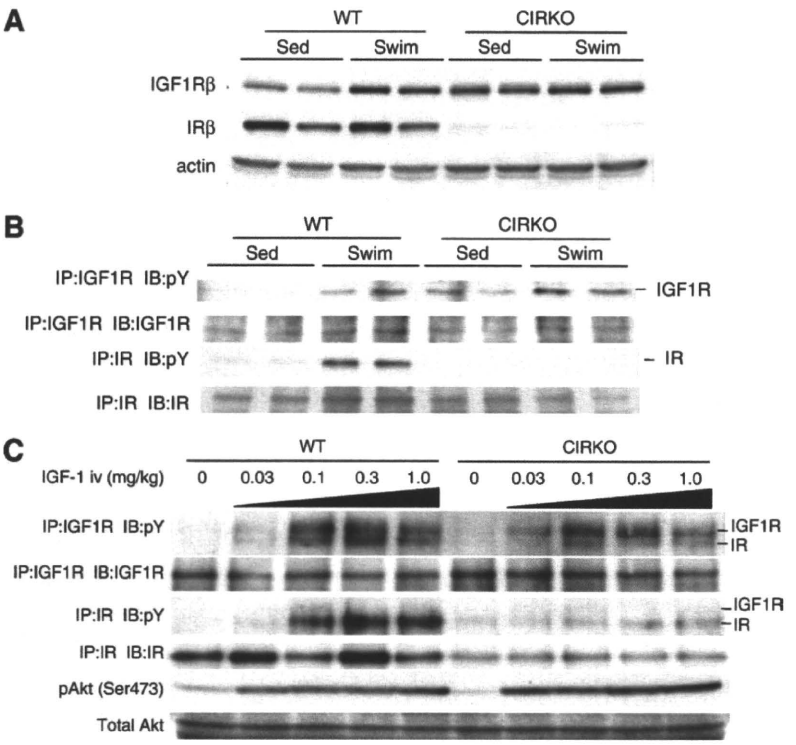

Fig. 5. Western blot analysis of CIRKO heart extracts after exercise or IGF-1 administration. (A) Expression of IGF1R β subunit protein (IGF1Rβ) and IR β subunit protein (IRβ) in the heart of WT and CIRKO mice. Sed and Swim represent a sedentary and a swimming group, respectively. (B) Tyrosine phosphorylation levels of IGF1R an IR following exercise training. pY represents anti-phosphotyrosine antibody. IP and IB represent immunoprecipitation and immunoblot, respectively. (C) Tyrosine phosphorylation levels of IGF1R/IR and activation of Akt in the heart of WT and CIRKO mice 5 minutes after IGF-1 administration. There are some IGF1R bands in the immunoprecipitates of IR and vice versa, possibly due to antibody cross-reactivity. pY represents anti-phosphotyrosine antibody. IP and IB represent immunoprecipitation and immunoblot, respectively.

moderately reduced (Fig. 7B, middle panel). Phospho-Akt levels in the heart were comparable between WT and IGF1R−/−IR+/− animals (Fig. 7B, lower panel).

In contrast to IGF1R−/−IR+/− mice, IGF1R+/−IR−/− mice exhibited small heart size at baseline, and the increase in HW and HW/BW ratio after 4 weeks of swimming was significantly reduced in IGF1R+/−IR−/− mice compared to WT mice (Figs. 8A–C). The increase in myocyte cross-sectional area was also markedly reduced in IGF1R+/−IR−/− animals compared to WT littermates (Figs. 8D and E). Echocardiography revealed a progressive decline in left ventricular contractile function in IGF1R+/−IR−/− mice, which was in part ameliorated by exercise training (Fig. 8F). Histological analysis demonstrated interstitial fibrosis in the heart of IGF1R+/−IR−/− mice at sedentary state, which was markedly reduced by exercise training (Fig. 8G). Western blot analysis of whole heart extracts revealed that the expression levels of IGF1R were upregulated in IGF1R+/−IR−/− hearts at sedentary state but there was no further upregulation of IGF1R expression after swimming (Fig. 9A). When IGF-1 was intravenously administered, tyrosine phosphorylation of IGF1R was moderately reduced (Fig. 9B, upper panel), and that of IR was markedly reduced (Fig. 9B, middle panel). Phospho-Akt levels in the heart were also reduced in the heart of IGF1R+/−IR−/− animals compared to WT mice (Fig. 9B, lower panel). These observations indicate that IR expressed from a single *Ir* allele is sufficient to

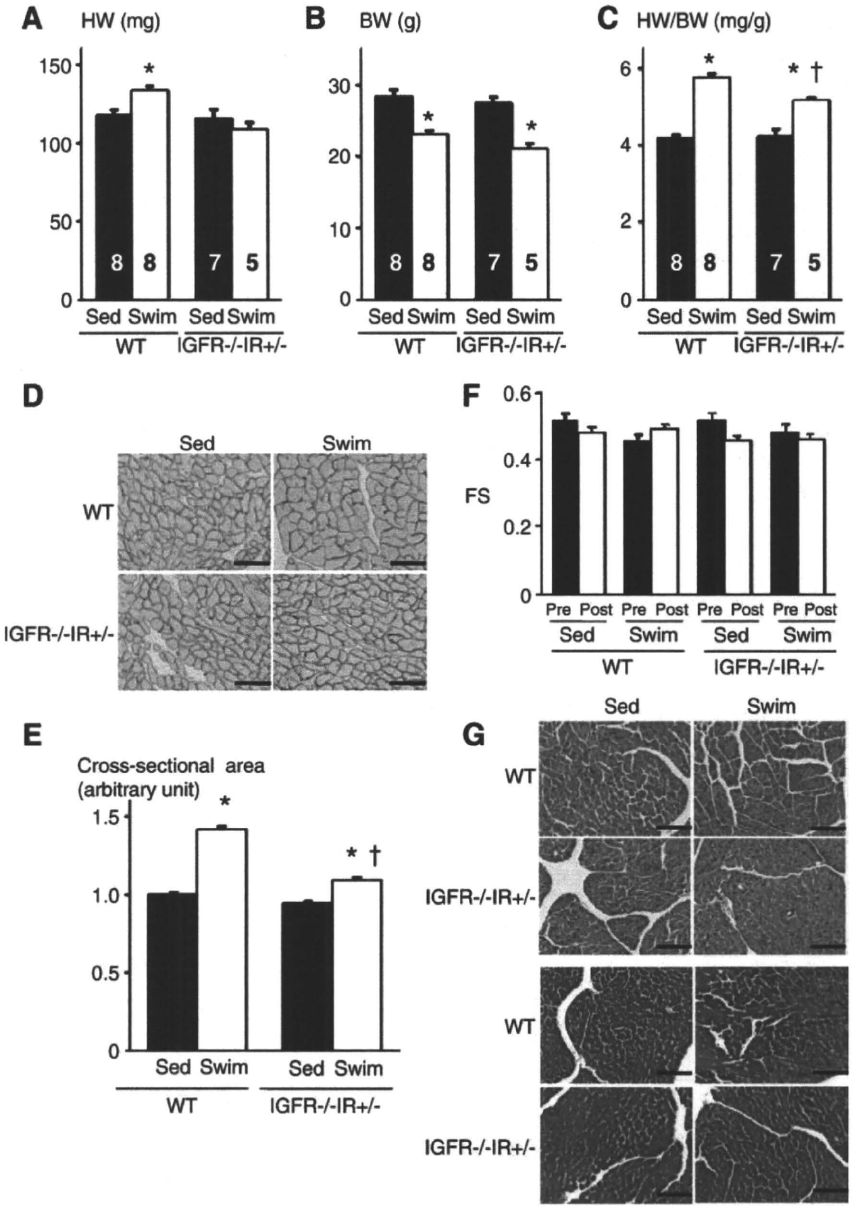

Fig. 6. Exercise-induced physiological cardiac hypertrophy is attenuated in IGF1R−/−IR+/− mice. (A–C) HW (A), BW (B), and HW/BW ratio (C) of WT and IGF1R−/−IR+/− mice. *p<0.05 versus Sed group of the same genotype, †p<0.05 versus WT Swim group. The number of mice analyzed is shown in the bar. (D) Immunohistochemistry with anti-dystrophin antibody. Scale bar = 50 μm. (E) Myocyte cross-sectional area of WT and IGF1R−/−IR+/− mice. *p<0.05 versus Sed group of the same genotype. †p<0.05 versus WT Swim group. (F) Left ventricular contractile function as assessed by echocardiographic measurement of fractional shortening (FS). Pre and Post represent before and after exercise, respectively. (G) Histological analysis with HE (upper panel) and Masson's trichrome (MT) (lower panel) staining. Scale bar = 100 μm. Sed and Swim represent a sedentary and a swimming group, respectively.

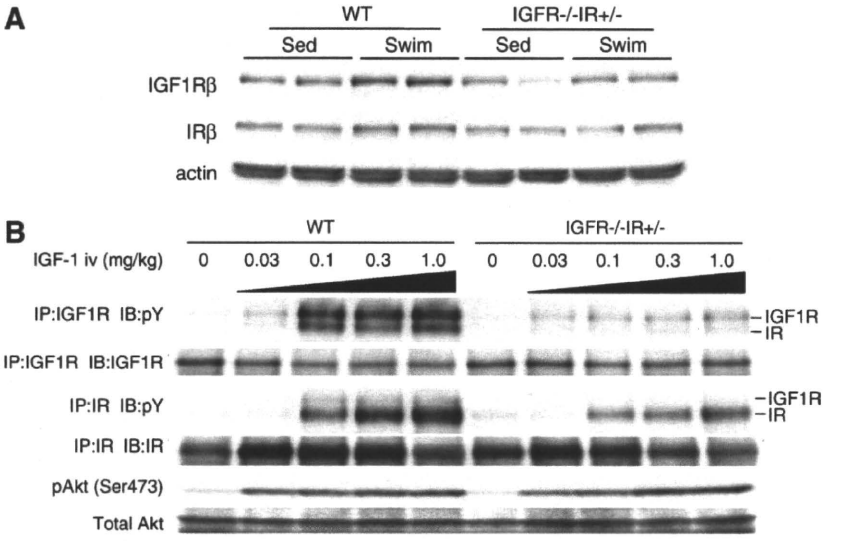

Fig. 7. Western Blot analysis of IGF1R−/−IR+/− heart extracts after exercise or IGF-1 administration. (A) Expression of IGF1R β subunit protein (IGF1Rβ) and IR β subunit protein (IRβ) in the heart of WT and IGF1R−/−IR+/− mice. Sed and Swim represent a sedentary and a swimming group, respectively. (B) Tyrosine phosphorylation levels of IGF1R/IR and activation of Akt in the heart of WT and IGF1R−/−IR+/− mice 5 minutes after IGF-1 administration. There are some IGF1R bands in the immunoprecipitates of IR and vice versa, possibly due to antibody cross-reactivity. pY represents anti-phosphotyrosine antibody. IP and IB represent immunoprecipitation and immunoblot, respectively.

maintain normal postnatal cardiac growth but is insufficient to support the full program of hypertrophic responses to exercise training, whereas IGF1R derived from a single *Igf1r* allele is insufficient both for the maintenance of postnatal cardiac growth/function and for the development of exercise-induced physiological cardiac hypertrophy.

4. Discussion

In the present study, we have dissected the roles of IGF1R and IR in normal postnatal cardiac growth and exercise-induced cardiac hypertrophy. We found that IGF1R and IR have overlapping or redundant functions in these two processes of physiological cardiac growth. We also found that both IGF1R and IR are activated by IGF-1 or exercise, implying that IGF1R- and IR-mediated signals could contribute to hypertrophic responses of the heart to exercise training. These results suggest the existence of a complex signaling network involving IGF1R, IR, and their ligands in the regulation and maintenance of cardiac growth and function (Fig. 10).

Biological actions of insulin and IGF-1 are transduced by IR and IGF1R. These receptors are highly homologous and exist as $\alpha_2\beta_2$ heterodimers, with two extracellular ligand-binding α subunits and two transmembrane β subunits that contain tyrosine kinase domains [28]. There also exists a hybrid IR–IGF1R receptor formed by IR α–β heterodimer and IGF1R α–β heterodimer, which preferentially binds to IGF-1 but not to insulin [29]. Under normal conditions, insulin and IGF-1 signal primarily through their cognate receptors. Thus, insulin signaling acutely regulates glucose metabolism, whereas IGF-1 signaling regulates embryonic and postnatal body/organ size. This notion is supported by distinct phenotypes of IR and IGF1R knockout mice: IR-deficient mice are perinatally lethal due to severe ketoacidosis, whereas IGF1R-deficient mice exhibit severe growth retardation (~45% of normal size) [30]. However, it is probably an oversimplification to view that IR mediates metabolic actions and IGF1R mediates growth. Indeed, IR-deficient mice are slightly smaller than wild type mice (~90% of normal size), and combined deletion of IR and IGF1R results in more severe growth retardation (~30% of normal size) than IGF1R single deletion [30]. Thus, IR and IGF1R have functional redundancies in mediating growth promoting effects during embryonic development.

We previously reported that CIRKO mice exhibit a small heart phenotype (~80% of the wild type heart size). Based on the observation that IGF1R-deficient mice show more severe growth retardation than IR-deficient mice [30], we initially hypothesized that IGF1R-mediated signals would play a dominant role over IR-mediated signals in normal postnatal cardiac growth. However, we found that there was no obvious cardiac phenotype in CIGFRKO mice at baseline. Furthermore, simultaneous deletion of *Ir* and *Igf1r* in cardiac myocytes resulted in perinatal lethality with contractile dysfunction and reduced heart size (data not shown). These observations suggest that IR and IGF1R have functional redundancies in mediating postnatal cardiac growth and that IR plays a dominant role over IGF1R in this process. Although the basis for differential contribution of IR and IGF1R to embryonic development (IR<IGF1R) versus postnatal heart growth (IR>IGF1R) is not clear, it may be due to differences in relative expression levels of IR, IGF1R, and their ligands during embryonic versus postnatal development.

The lack of obvious cardiac phenotype in CIGFRKO mice prompted us to investigate the effect of *Igf1r* deletion in the heart under stressed conditions. Previous studies implicated a critical role of IGF-1–PI3K–Akt pathway in the development of exercise-induced physiological cardiac hypertrophy [9,10]. Specifically, gain-of-function studies in transgenic mice revealed that IGF1R is capable of inducing physiological cardiac growth [14]. We therefore hypothesized that hypertrophic responses to exercise training might be impaired in the heart of CIGFRKO mice. Unexpectedly, however, both wild type and CIGFRKO mice developed comparable levels of cardiac hypertrophy in response to swimming training. In addition, IGF-1 administration or exercise training induced extensive tyrosine phosphorylation of IR in the heart of wild type and CIGFRKO mice. On the contrary, insulin administration induced robust phosphorylation of IR but not IGF1R (Supplementary Fig. S3). These findings suggest that both IGF1R and IR can be activated by IGF-1 and may contribute to the development of exercise-induced cardiac hypertrophy in a functionally redundant fashion. This notion was further supported by our studies in CIRKO, IGF1R−/−IR+/−, and IGF1R+/−IR−/− mice, in which combined deletion of *Igf1r* and *Ir* gene in cardiac myocytes attenuated hypertrophic responses of the heart to exercise training whereas deletion of *Ir* gene alone did not. Furthermore, the observation that IGF1R+/−IR−/− mice were more severely impaired in hypertrophic

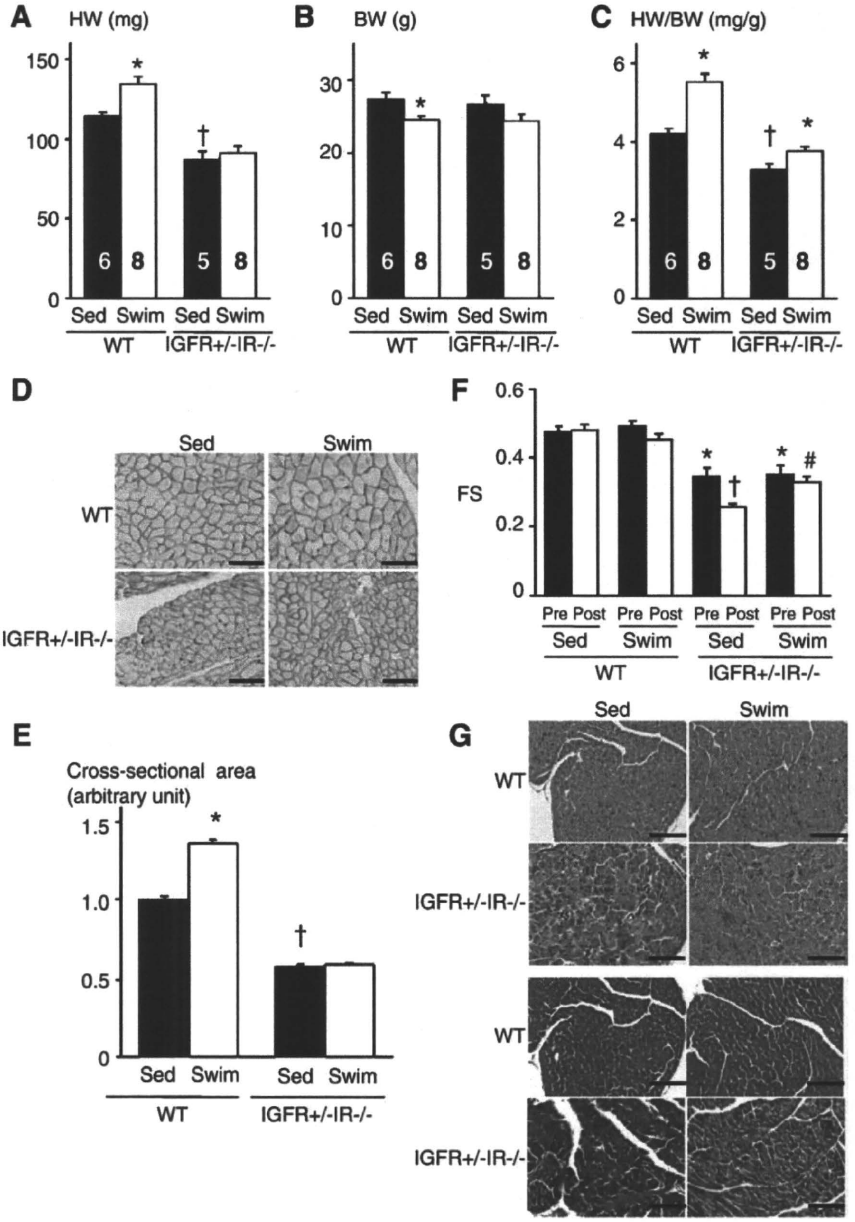

Fig. 8. Exercise-induced physiological cardiac hypertrophy is attenuated in IGF1R+/−IR−/− mice. (A–C) HW (A), BW (B), and HW/BW ratio (C) of WT and IGF1R+/−IR−/− mice. *p<0.05 versus Sed group of the same genotype, †p<0.05 versus WT Sed group. The number of mice analyzed is shown in the bar. (D) Immunohistochemistry with anti-dystrophin antibody. Scale bar = 50 μm. (E) Myocyte cross-sectional area of WT and IGF1R+/−IR−/− mice. *p<0.05 versus WT Sed group. †p<0.05 versus WT Sed group. (F) Left ventricular contractile function as assessed by echocardiographic measurement of fractional shortening (FS). Pre and Post represent before and after exercise, respectively. *p<0.05 versus WT Sed Pre group, †p<0.05 versus IGF1R+/−IR−/− Sed Pre group, #p<0.05 versus IGF1R+/−IR−/− Sed Post group. (G) Histological analysis with HE (upper panel) and Masson's trichrome (MT) (lower panel) staining. Scale bar = 100 μm. Sed and Swim represent a sedentary and a swimming group, respectively.

responses to exercise than IGF1R−/−IR+/− mice suggests that IR-mediated signals might play a dominant role over those mediated by IGF1R in exercise-induced cardiac hypertrophy, as is the case with normal postnatal cardiac growth. Our results also suggest the possibility that the small heart phenotype of CIRKO mice is in part due to the impairment of IR signals activated by IGF-1 or IGF-2 but not by insulin.

The IGF-1–PI3K–Akt pathway has been implicated in physiological cardiac growth. However, the precise mechanism by which this signaling pathway regulates cardiac growth is not completely understood. Although IR appears to be activated by IGF-1 in the heart, the binding affinity of IGF-1 to IR has been reported to be ~100-fold lower relative to that of insulin to IR. One possible mechanism of cross talk between IGF-1 and IR is the ability of IGF1R-IR hybrid receptors to bind to IGF-1 but not to insulin. It was also recently shown that IGF-1 activates IR at physiological concentrations in murine fibroblasts [31]. In this case, IGF-1 selectively activates IRS-2 and the PI3K pathway but not the IRS-1 and ERK pathway. These and other potential mechanisms of IR activation by IGF-1 could contribute to the development of exercise-induced cardiac hypertrophy.

Kim et al. [20] recently reported that exercise-induced cardiac hypertrophy is attenuated in CIGFRKO mice and that activation of AMPK in the heart of CIGFRKO mice is a potential mechanism leading to impaired hypertrophic responses in these animals. However, we could not detect significant differences in cardiac AMPK activity between WT and CIGFRKO mice either before or after exercise. An